U.PORTO
FACULDADE DE CIÊNCIAS
UNIVERSIDADE DO PORTO

MSc
2nd CYCLE
FCUP
2015

U.PORTO

Sensing for Structural Health Monitoring of Composite Laminates

Luís Duarte Pereirada Costa

FC

Sensing for Structural Health Monitoring of Composite Laminates

Luís Duarte Pereira da Costa

Master's Dissertation submitted to the Faculty of Sciences of the University of Porto in Engineering Physics

2015

U.PORTO
FACULDADE DE CIÊNCIAS
UNIVERSIDADE DO PORTO

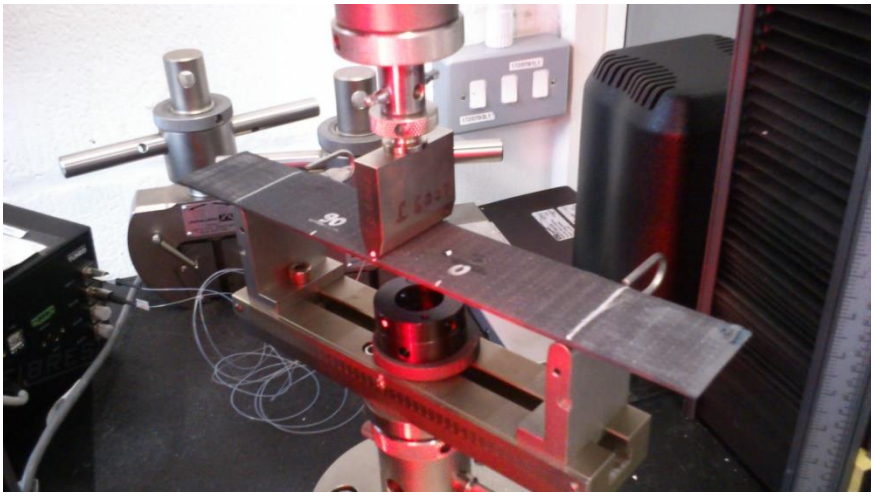

Sensing for Structural Health Monitoring of Composite Laminates

Luís Duarte Pereira da Costa

Integrated Masters in Engineering Physics

Department of Physics

2015

Supervisor

Orlando Frazão,Invited Assistant Professor, Faculty of Sciences of the University of Porto

Co-Supervisor

Matthieu Gresil, Lecture, School of Materials of the University of Manchester

All modifications determined by the Jury, and only those, were made.

The president of the Jury,

Porto, _____/_____/_____

“Really, the only thing that makes sense is to strive for greater collective enlightenment.”

Elon Musk

Sensing for Structural Health Monitoring of Composite Laminates

Luis Costa

Abstract

This work focuses on the development of smart materials, by embedding FBGs in composite plates. A sensor head in composite was developed, with the ability to monitor it's own cure and of simultaneous measurement of curvature and temperature or strain and temperature, in real time. The performance of the FBGs as acoustic sensors for the detection of defects in the material is also evaluated. The embedding methods of the sensors in the material were studied and a hybrid composite plate was designed (with unidirectional and bidirectional sections), with FBGs embedded in each section. The different properties of the material in each section produce variations in each of the FBGs sensitivities, enabling simultaneous measurement.

Before the fabrication, the design of the plate was evaluated through finite element simulations (*ABAQUS-CAE*), which were then compared to the mechanical characterization of the sample. The cure monitoring showed the glass transition and the quantification of the residual strains produced in each of the sections after the cure. After the manufacture, the sensor response was characterized, as well as the sensitivity change due to the embedding process and cure, which allowed the development of the sensor matrix for simultaneous measurement. For damage detection, the dispersion curves of the plate were numerically obtained, being afterwards the FBG response compared with the numerically obtained values and piezoelectrics. The directionality of the FBG was also studied, showing higher sensitivity to longitudinal emissions than transverse. The FBG behavior was similar to that of the piezoelectrics, although it presented higher sensitivity to the wave's A0 mode. A simulated defect was introduced, and the ideal conditions for it's detection were determined. The FBG was able to detect it up to 10 degrees off axis (emitter-receiver).

Sensing for Structural Health Monitoring of Composite Laminates

Luis Costa

Resumo

Este trabalho foca-se no desenvolvimento de materiais inteligentes, embutindo FBGs em placas de compósito. Foi desenvolvida uma cabeça de sensor, em compósito, capaz de monitorizar a sua cura e de medição simultânea de temperatura e curvatura ou deformação e temperatura em tempo real. O desempenho dos FBG como sensores acústicos para deteção de defeitos no material é também avaliado. Os métodos de introdução dos sensores no material foram estudados e foi desenhada uma placa de compósito híbrida (com secções unidirecional e bidirecional), com FBGs embutidos em cada secção. As diferentes características do material em cada secção proporcionam variações nas sensibilidades locais do FBG, possibilitando a medição simultânea.

Antes da fabricação, o desenho da placa foi avaliado recorrendo a simulações de elementos finitos (*ABAQUS-CAE*), posteriormente comparados à caracterização mecânica da amostra. A monitorização da cura levou à verificação da transição vítrea e quantificação da deformação residual existente nas secções da amostra após a cura. Após a fabricação, a resposta dos sensores foi caracterizada, bem como a variação da sensibilidade proveniente da introdução no material, levando ao desenvolvimento da matriz de medição simultânea para a cabeça de sensor. Para o efeito de deteção de defeitos, as curvas de dispersão da placa foram calculadas numericamente, sendo depois a resposta dos FBG comparada com os valores obtidos numericamente e com piezoeléctricos. A direccionalidade do FBG foi também estudada, verificando-se ser mais sensível a emissões longitudinais do que a transversais. A resposta do FBG mostrou-se semelhante à do piezoeléctrico, apesar de se mostrar mais sensível ao modo A0 da onda. Um defeito simulado foi introduzido e foram estudadas quais as condições ideais para a sua deteção. O FBG foi capaz de detetá-lo até 10 graus fora da linha emissor-recetor.

Acknowledgements

Several people contributed, directly or otherwise, to the realization of this work. To all of them, I wish to express my sincere gratitude.

I would like to express my gratitude to my supervisors, Dr. Orlando Frazão and Dr. Matthieu Gresil, for the patience, the support, expertise and guidance which were incredibly valuable for my graduate work. The opportunity to work abroad in such an incredible research environment was invaluable to my personal and academic growth, and is very much appreciated.

I wish to express my sincere thanks to Dr. Costas Soutis, the Director of Northwest Composites Centre and NCCEF, for welcoming me at the University of Manchester, and providing the necessary facilities and infrastructure for the research.

I would also like to thank all of the labmates and staff at NCCEF, in Manchester for being so welcoming and supportive throughout my time there, and for all the advice even as I struggled to introduce myself to new research topics and subjects. I would also like to thank Dr. Clara Frias for the shared knowledge and experience.

To all the Center for Applied Photonics of INESC-TEC staff and researchers, a kind word for being always supportive and eager to assist in any way towards the conclusion of this work. Thank you for embracing me as part of your team.

A very warm and special thanks goes out to all of my incredible friends and family, for keeping me company even when I was away, for all the advice and support in the times of most discouragement, and for the much-needed joy they brought throughout all these years. You taught me a lot, and you have all made me who I am right now.

I am also thankful to Regina, for being so supportive and caring regardless of the distance and time, and greeting me with laughter day after day.

Lastly, I'd like to thank my amazing family: My brilliant twin brother, João, for all the help, the positivity, and for always providing an example and inspiration of someone I should strive to be, and my parents, João and Deolinda, whose ceaseless support and education brought me to where I am right now, and to whom I'm forever grateful for fostering my potential and leading me this far. I couldn't have wished for better parents, and I seek to make you proud.

Contents

List of Figures

List of Tables

Abbreviations

AVE	**A**dvanced **V**ideo **E**xtensometer
CF	**C**arbon **F**iber
CFRP	**C**arbon **F**iber **R**einforced **P**olymer
DOFS	**D**istributed **O**ptical **F**iber **S**ensors
DSC	**D**ifferential **S**canning **C**alorimetry
EFPI	**E**xtrinsic **F**abry-**P**érot **I**nterferometer
EMI	**E**lectro**M**agnetic **I**nterference
FBG	**F**iber **B**ragg **G**rating
FE	**F**inite **E**lements
FP	**F**abry-**P**érot
FRP	**F**iber **R**einforced **P**olymer
FTIR	**F**rustrated **T**otal **I**nternal **R**eflection
GFPC	**G**rating **F**abry- **P**érot **C**avity
IR	**I**nfra**R**ed
LPG	**L**ong **P**eriod **G**rating
NDE	**N**on **D**estructive **E**valuation
NDT	**N**on **D**estructive **T**esting
PTFE	**P**oly**T**etra**F**luoro**E**thylene (Teflon)
PVDF	**P**oly**V**inyli**D**ened**F**loride
PZT	Lead Zirconate Titanate (Piezoelectric Crystal)
SHM	**S**tructural **H**ealth **M**onitoring
TDM	**T**ime **D**ivision **M**ultiplexing
UV	**U**ltra**V**iolet
WDM	**W**avelength **D**ivision **M**ultiplexing

To my beloved parents, João and Deolinda.

Part I

Preface

CHAPTER 1

Introduction

1.1 Motivation

The need to overcome material-imposed limitations on new techniques and technologies has led to an interest in composite materials for both industrial and research purposes. By appropriately choosing the matrix and reinforcement materials and controlling their orientation, manufacturers can tailor the material with the required properties, anisotropy and environmental resistance (i.e. against corrosion, acidity, temperature, among others) for any particular purpose and structure, achieving high performance and high cost-efficiency for each specific application. Nowadays, composites show relevance in several fields, such as military, civil engineering and aerospace, motor sports, consumer products (e.g. skis, golf clubs, rackets), among others where the strength-to-weight ratio and the ability to withstand environmental and work conditions are pivotal to the safe use of the part and/or lead to savings in operation cost over the course of the material life.

Due to their newfound broad use and interest, the study of new non-destructive testing (NDT) and structural health monitoring techniques (SHM) for composite parts, or the adaptation of previously used techniques for other kinds of materials becomes increasingly relevant. While the material is in operation, being able to assess its status in a non-intrusive, non-destructive way, in-situ and in real time can be of critical importance. Premature maintenance or replacements are cost inefficient and lead to unnecessary downtime. Conversely, neglecting maintenance and repairs can lead to catastrophic failure. Non-destructive evaluation (NDE) systems integration prevents both kinds of issues, while improving the safety, reliability and optimizing manufacturing yields.

This addition of embedded sensing capabilities leads to the creation of so-called ”Smart Materials”, able to report changes in their state, warning the user as soon as the material reaches a precarious state, or reacting to its alteration through embedded actuators.

Optical fiber sensors stand out due to their sensing capabilities while being less intrusive than copper wire, immunity to electromagnetic interference and lack of resistive heating through Joule effect, effectively producing minimal influence in the material properties after embedding [1–3]. These sensors can be intrinsic or extrinsic, sensing alteration to the surrounding environment by measuring changes in phase, intensity, wavelength, polarization or transit time. Intrinsic sensors, in particular, are interesting as these are often easily multiplexed, providing sensing over large distances [4]. In particular, fiber Bragg gratings have been extensively studied and show promising results as embedded sensors for composite materials and structures [5] due to their ease in multiplexing [6] and cost efficiency, having in previous studies been shown to allow monitoring of the material from the manufacturing process [7–9] to in-situ measurements of strain and temperature [10–12], damage detection [13–15] and evaluation of patch repairs [16].

The conducted work intends to assess the viability of fiber Bragg gratings for structural health monitoring and non-destructive testing of composites, addressing the techniques and considerations for the manufacture of plates with embedded optical sensors. Afterwards, it presents the setups, procedures and results of the same FBGs for manufacture monitoring, in-situ monitoring of physical parameters (strain/temperature and curvature/temperature) and detection of damage. The end purpose is to validate the presented new designs and sensors as an alternative to other previously established methods of monitoring and evaluation for composite materials, as these become increasingly ubiquitous.

1.2 Objectives

- Manufacture a carbon fiber reinforced polymer (CFRP) plate with a unidirectional and bidirectional sections each with a embedded fiber Bragg grating using vacuum assisted resin infusion.
  - Assess methods of embedding and accessing the sensors.
  - Monitor the manufacture of the same plate using FBG sensors, specifically the cure process, and observe the glass transition and final residual strains of the plate for both each section. Evaluate the influence of the process in the ultimate sensor’s response.

  - Measure the response of the same sensors to strain, temperature and curvature, and compare the results to prediction models made using finite element simulations.
  - Create a sensor head capable of simultaneous measurements of strain/temperature and curvature/temperature using the aforementioned plate.

- Assess the viability of fiber Bragg gratings as transducers for the non-destructive evaluation of a quasi-isotropic CFRP plate using guided Lamb waves.

  - Design the experimental setup with embedded fiber Bragg grating and piezoelectric sensors, capable of the acquisition of high frequency acoustic waves.
  - Correlate the measured group velocities to those estimated numerically using both piezoelectric and fiber Bragg grating sensors.
  - Compare the FBG and piezoelectric amplitude response as a function of frequency to the first symmetric and anti-symmetric modes of propagation.
  - Study the FBG response for acoustic waves emitted longitudinally and transverse to the fiber's orientation.
  - Analyze the sensitivity to damage/defect of both the piezoelectrics and fiber Bragg gratings, as a function of frequency and relative position of the defect.

1.3 Structure of the dissertation

The first chapter introduces this work's motivation and purpose, establishing the context and relevance of the research. It follows by summing up the proposed objectives for the work and its structure and the resulting outputs and publications.

The second chapter consists of a theoretical introduction to composite materials fundamentals, macro and micromechanics and a description of the used type of composites.

The third chapter introduces the transducers used for structural health monitoring and non-destructive testing. It develops the fundamentals of optical single mode fibers and optical fiber sensors, then focuses on fiber Bragg gratings, to explain the principles of work, history, fabrication and methods of interrogation and multiplexing.

The fourth chapter combines the concepts of the previous chapters to introduce the concept of "Smart materials". It follows with a state-of-the-art of the studies relevant to the influence of optical fibers to the host material properties, cure monitoring, in-situ real-time monitoring of strain and temperature using FBG, and acoustic damage

detection. It also briefly explains guided Lamb waves and the principles of ultrasonic acoustic wave damage detection methods.

The fifth chapter focuses on the uses of the sensors and the experiments for the purpose of structural health monitoring and monitoring of the manufacture, with an explanation and report of the plate design, lay-up and manufacture and subsequent finite element analysis. The theory for the design of the sensor head is then exposed. The reader is then presented with the analysis of the experimental results for the monitoring of the manufacture, the temperature, strain and curvature characterization of the embedded sensors and comparisons with the aforementioned simulations, and the development of the sensor matrix for simultaneous measurement of temperature/strain and temperature/curvature.

The sixth chapter delves with non-destructive evaluation techniques of composite plates, namely guided Lamb waves. The chapter describes the experimental setup and the plate used for the damage detection, with an explanation of the techniques for measurement using the fiber Bragg grating and the signal processing applied to the acquired signals. FBG and piezoelectric response is then compared to the theoretical estimated values of the group velocity and the modes of propagation measured are identified, and the amplitude of each is measured as a function of the frequency used. The chapter finishes with the detection of a simulated defect using the same setup.

The final chapter ends with a conclusion and overview of all the results, a discussion and comments on possible future work.

1.4 Outputs

Published journal paper to *Smart Materials and Structures*:

L. Costa, M. Gresil and O. Frazão,“Simultaneous measurement of physical parameters using FBG embedded in unidirectional and bidirectional composite materials”, *Smart Materials and Structures*, 2015 *(pending acceptance)*

Part II

Fundamentals and State of the art

CHAPTER 2

Composite Materials

Structural materials can be divided into four basic categories : metals, polymers, ceramics and composites. This work's focus is on the latter, which consist of any sort of macroscopic, heterogeneous combination of the remaining three types.

Whenever the structural unit is microscopic, however, the material is not commonly known as a composite (such is the case of alloys or polymer blends), being the definition reserved to the macroscopically heterogeneous case [17]. This is a broad definition, encompassing for instance plywood and reinforced concrete. More specifically, this work attends to fiber-reinforced composite materials. As a heterogeneous combination of materials, the constituents of a composite are discriminated as reinforcement and matrix, both being physically and chemically distinct, with a clear interface, having the final part's behavior dependent on both constituents and the interface properties.

These materials provide several advantages, such as high fatigue resistance and strength, high specific properties per unit weight, good longevity when compared to analogous monolithic materials, and control of anisotropy and ply configurations for selective reinforcement, for carrying combinations of axial and shear loads to suit the application. In principle, composites can be tailored to achieve optimum properties for each application, and recent improvements in simulated models allow better prediction of the behavior of each part even after the manufacturing.

Until 1975, fiber-reinforced composites were mainly produced at a laboratory scale [18]. Nowadays, the increasing demand of specific properties per unit weight, higher resistance to environmental conditions to enable more sophisticated engineering and lower operation costs has led several industries to make composite technology a standard in several of their products and equipment. Such is the case of modern aerospace: New designs for aircrafts/turbines are useless without adequate materials, able to withstand the workload and environment while meeting the weight requirements.

2.1 Fiber Reinforced Polymer Composites

While a composite can be defined as any heterogeneous mixture of two materials with a macroscopic unit cell, one particularly common and relevant case is that of fiber reinforced polymer (also known as fiber reinforced plastic) composites (FRP). These consist of polymers which make use of other materials in fiber form as reinforcement to enhance the mechanical properties of the plastic. When they are formed as a stack of lamina, the composite is called a laminate, as represented in Figure 2.1.

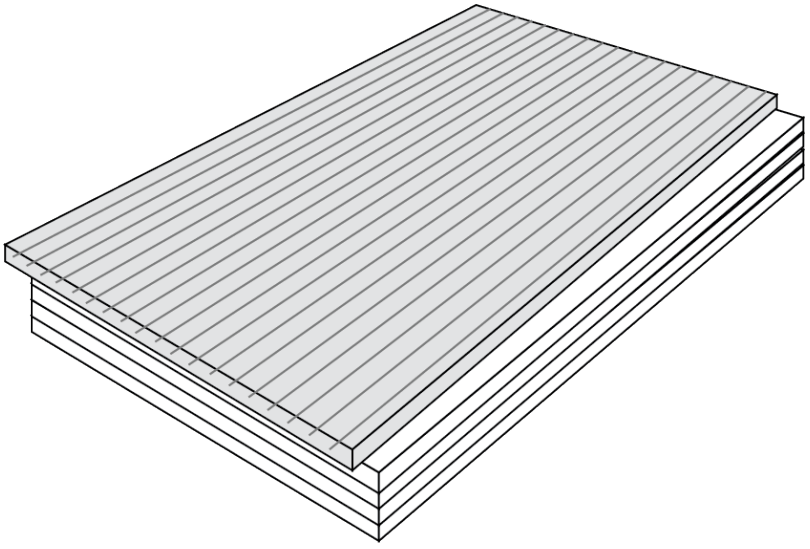

FIGURE 2.1: Scheme of composite laminate, consisting of a stack of laminae.

Frequently, the fibrous reinforcement is composed of continuous fibers of carbon, aramid or glass. The prominence of these kinds of fiber reinforced composites derives from the high-aspect ratio resulting from the fiber geometry, which makes most materials stronger and stiffer along the fiber direction, and materials in general are stronger while in fiber form. Fibers, however, buckle under the application of longitudinal compressive loads and have poor transverse mechanical properties. Therefore, the matrix has the very important role of connecting them in a structural unit, as in spite of their properties, fibers alone are generally useless as a structural material unless held together.

Most commonly, the matrix is a resin, such as a polyester, vinyl ester or epoxy, but it can also take the form of several other kinds of polymers (Polymer Matrix Composites - PMC), metals (Metal Matrix Composites - MMC) or ceramics (Ceramic Matrix Composites - CMC) [19]. The ability of the matrix to transfer the load to the neighboring fibers is inherently associated with the size of the interface of both constituents. In consequence, the fibrous geometry of the reinforcement is also advantageous as it produces a high surface area in relation to the volume of each fiber. The aspect ratio of a fiber is found to be:

$$\frac{\text{Area}}{\text{Volume}} = \frac{2\pi rl}{\pi r^2 l} = 2/r \tag{2.1}$$

thus, fibers with a very small radius create a proportionally sizable interface for stress transfer, ensuring that a large fraction of the load can be easily distributed to all the other surrounding fibers through the matrix [20].

The resulting composite uses the matrix material (polymer) to transfer the load through the matrix and distribute it to all the reinforcing fibers, to prevent fiber buckling (which allows the fibers to carry compressive loads) and to enhance the transverse properties of the material, compared to the reinforcement alone. As such, although it is not the primary loading component, by distributing the load through the reinforcement, the matrix is crucial to the material's end properties, with the added purpose of keeping the fibers in place and protecting them from moisture and other environmental hazards.

The final composite's properties can be ultimately tailored, by changing the materials used as reinforcement and matrix, their respective volume fractions and the geometry/orientations of fibers in the composite. The combination of matrix and reinforcement results in mechanical properties exceeding the matrix alone, taking advantage of the reinforcing fibers' high tensile properties. Different combinations of the fiber orientations and geometry assembled in a sheet lead to many different type of fabrics, with varying specific characteristics. The fabric geometries can be unidirectional, bidirectional (*e.g.* woven, twill, etc.) or even some 3D designs with more reinforcement through the thickness, all with varying patterns to achieve different directional properties [21].

2.1.1 Carbon fibers

Carbon fibers (CF) possess very high strength-to-weight and stiffness-to-weight ratio, low thermal expansion, and high fatigue resistance, making them ideal for applications where weight is critical while maintaining high strength.

Typically, CF possess very anisotropic properties, and can be acquired with a range of varying tensile properties and ultimate strength owing to their microscopical arrangement of atoms. High-strength carbon fibers, such as IM10 and T-1000G have been known to reach tensile strength more than six times that of steel. These type of fibers are often made of radius ranging from 9 to 17 μm.

2.1.2 Polymer Matrix

When picking the matrix properties such as the ductility, toughness and electrical insulation are often considered. In order to produce a strong interface, the matrix should also be chemically compatible with the reinforcement, which involves being able to produce a chemical bond with the reinforcing fibers without any undesirable reactions occuring at the interface, in the case of high-temperature composites.

The first consideration when choosing a matrix, as such, is the service temperature. Polymers are currently the most commonly used matrix materials. These can be divided into thermosets (*e.g.* epoxies) or thermoplastics (*e.g.* polyamide). The former, after curing, produce polymer chains that do not soften/melt at high temperatures, as opposed to the latter [17].

2.2 Fabrication Process

Several techniques are used for the manufacture composite plates. Considerations must be taken when deciding which technique to use, such as cost, available infrastructure, the geometry and size of the sample, choice of reinforcement and matrix, and desired finish. Some techniques are more prone to variations or susceptible to the skill of the worker, being overall less consistent in the final quality, volume fractions and amount of voids present in the part, which should also be taken into consideration.

The reinforcement can either be set in place using bundles or individual fibers through filament winding or by being arranged into a form of sheet, known as fabric, to make the handling and stacking (for some kinds of structures, such as plates) easier. As a summary, this work will reference the most common fabrication methods used for polymer matrix composite plates, using fabric sheets for the layup [17]:

Hand Layup Although nowadays it is not a common method for the manufacture of composite plates, being more reserved for large structures or prototypes, it is a relevant mention as the oldest and simplest method. It involves intensive labor and is very time consuming, being more suited for larger components.

The resin is impregnated by hand into the reinforcement using rollers/brushes. Air voids are removed manually by squeezing and rolling out the air. It is most often used with room-temperature curing resins as matrix. This method presents inconsistent results in quality, dependent on the skill of the person doing the layup, but the tools are often cheaper and it is more easily available.

Vacuum Assisted Resin Infusion is another common method, where a bag is used to create and keep the sample in vacuum. The bag will have an inlet for the resin and an vacuum pump outlet on opposite sides of the laminate. Keeping the laminate in vacuum, with bagging film, pressures and compresses the fabrics. Usually a mesh is used to improve the flow of resin, separated from the laminate using a peel ply to be ripped afterwards. Due to the pressure gradient created by the vacuum pump, resin flows across and through the laminate from the resin inlet to the vacuum outlet.

It offers lower void content than hand lay-up, although it introduces extra costs involved in the bagging materials.

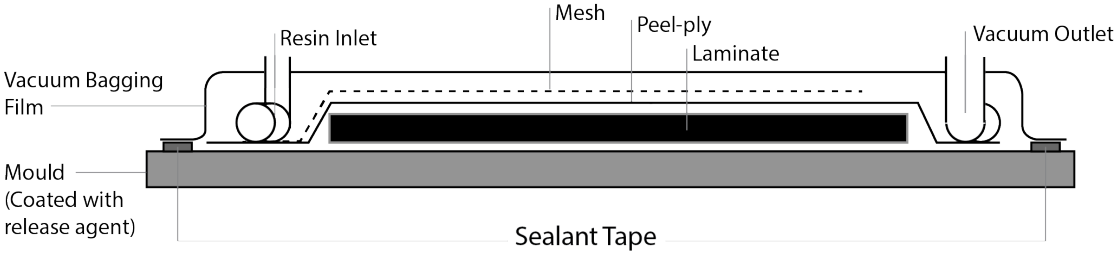

FIGURE 2.2: Vacuum assisted resin infusion set-up.

Prepreg Fabrics/Autoclave molding This method uses "prepreg" fabrics, which are pre-impregnated with resin. Usually, the impregnated resin does not cure at room temperature, so the lamina can be kept for a very long time, which can further be prolonged by keeping them at lower temperatures. These can be easily shaped and vacuum bagged (without need for a resin inlet), and then cured in an oven. This method doesn't require as much skill and can be more easily automated, and offers consistent properties and fiber volume fractions even without a skilled operator. However, the materials are more costly, and often an autoclave is required for the manufacturing as the standard way to use prepreg is by autoclave molding, since the high cost of the higher quality raw materials justifies the use of the higher quality techniques.

An autoclave is essentially a heated pressure vessel. The prepreg bagged mold is placed inside the autoclave at the required pressure and temperature settings for the curing cycle. A vacuum outlet is also created for the bag, removing any volatile gases produced during the cure, leading to a very low void content). This method produces the highest quality materials and the most predictable properties. However, the size of the final part is limited to that of the autoclave, and the high cost and energy consumption of the autoclave and prepreg fabrics is limiting for some applications.

For polymer matrix composites, the American Society for Testing and Materials (ASTM) standard for measurement of the volume fractions of resin and fiber involve two methods [22]: The first, after the manufacture, is that of acid digestion (for carbon fibers), or resin burn-off (for glass fibers). The second is by assuming that the fiber weight per unit area is known to an acceptable degree, and by measuring the thickness of the laminate [17].

This work uses vacuum assisted resin infusion for all the manufactured samples, and all samples use unidirectional carbon fabrics for the lay-up. The volume fraction is estimated by previous calculation of the volume of resin required to be infused in the composite preform. For better yields in sensor applications for composite plates, however, prepreg is often used as the standard in other studies. This method minimizes the need of sawing and cutting the sample after the cure, guarantees very predictable volume fractions of fiber/epoxy and facilitates handling during the manufacturing (simplifying the placement of the sensors at exact places). It also minimizes the influence of the sensor embedding in the local properties of the composite since there is no need for weaving the optical fiber through the fabric material.

2.3 Basic concepts of micro and macromechanics of composites

Composites differ from other kinds of materials, in the sense that the local behavior of the structure will differ from the gross mechanical behavior of the overall part. The overall behavior may be characterized by averaging stresses/strains to obtain effective mechanical properties of an equivalent homogeneous material. Other materials may be homogeneous and isotropic, so the local properties remain constant throughout the material and are independent of the orientation. Composites, on the other hand, have different properties in matrix and fiber, which also depend on the orientation. As such, relationships between stresses and strains are much more complicated in the case of composites, due to coupling effects (*i.e.* a normal stress may induce normal and shear strains, thermal expansion is not uniform and creates distortions, etc.).

Therefore, the study of composites has to be done both from a microscopic and a macroscopic perspective. A micromechanical analysis of composites intends to predict the response of the heterogeneous combination of materials, based on the individual properties of the matrix and reinforcement, and evaluate the local stress and strain response of the material. Study of the microscopic properties are useful to understand failure mechanisms and elastic properties but are impractical for the study of large structures as

they impose high computational costs. In general, the focus of a micromechanical analysis is on effectively establishing the relationships between the each of the constituent's properties, and the effective properties for the composite.

As a rough estimation, one can use the "rule-of-mixtures" to get an approximation of the properties of the material by calculating the final properties from the matrix and reinforcement individual properties and their respective volume fraction. The obtained "effective" or "homogenized" properties lead to a simplification of the problems by then considering the composite a homogeneous material of the same geometry and with the calculated effective properties. These properties are estimated for a representative volume element (or unit cell), and then extrapolated for the whole material.

This approach makes an assumption of perfect bonding between fiber and matrix, essentially neglecting effects of the interface.

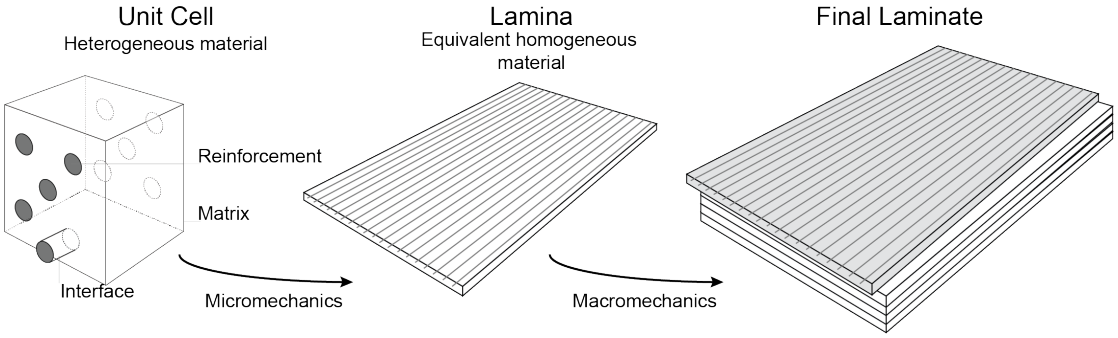

FIGURE 2.3: Representation of the micromechanical to macromechanical analysis procedure.

The first distinction to be made regarding the heterogeneous nature of the composite is the relative amount of each of the components. This is defined by the volume fractions which alone directly enable the computation of properties such as the density of the composite, by assuming no volume occupied by voids.

$$\frac{\text{Volume of fiber} + \text{Volume of matrix}}{\text{Total volume}} = V_f + V_m = 1 \tag{2.2}$$

The rule of mixtures is generally defined as the weighted average of the properties of each component. For estimations of the final part's modulus, in general, two basic models can be distinguished: Voigt model, for axial loading and Reuss model, for transverse loading **??**. Voigt model assumes an equal strain condition

$$\varepsilon_1 = \varepsilon_{1f} = \frac{\sigma_{1f}}{E_f} = \varepsilon_{1m} = \frac{\sigma_{1m}}{E_m} = \frac{\sigma_1}{E_1} \tag{2.3}$$

ε_1 and σ_1 being the strain and stress along the longitudinal direction, and the subscript m and f referring to matrix and fiber, respectively.

Reuss model assumes an equal stress condition, so the stress acting on the reinforcement is equal to that on the matrix

$$\sigma_2 = \sigma_{2f} = \varepsilon_{2f} E_f = \sigma_{2m} = \varepsilon_{2m} E_m \tag{2.4}$$

ε_2 and σ_2 being the strain and stress along the transverse direction.

From the equations 2.3 and 2.4 comes

$$\sigma_1 = (1 - V_f)\sigma_{1m} + V_f \sigma_{1f} \tag{2.5}$$

$$E_1 = \frac{\sigma_1}{\varepsilon_1} = \frac{(1 - V_f)\sigma_{1m} + V_f \sigma_{1f}}{(\frac{\sigma_{1f}}{E_f})} = (1 - V_f)E_{1m} + V_f E_{1f} \tag{2.6}$$

E_1 being the longitudinal modulus and V the fiber volume fraction, $(1-V_f)$ consequently being the matrix volume fraction.

$$\varepsilon_2 = V_f \varepsilon_{2f} + (1 - V_f)\varepsilon_{2m} \tag{2.7}$$

$$E_2 = \frac{\sigma_2}{\varepsilon_2} = \frac{\sigma_2}{V_f \varepsilon_{2f} + (1 - V_f)\varepsilon_{2m}} = [\frac{V_f}{E_f} + \frac{(1 - V_f)}{E_m}]^{-1} \tag{2.8}$$

E_2 being the transverse modulus. It is shown to be a matrix-dominated property, as the influence of the fibers on the final value is exceptionally low unless for outstandingly high values of V_f.

The transverse model is the worse estimation of the two, as the strain distribution is essentially homogeneous during axial loading, but not during transverse, during which an equal stress assumption is incorrect due to the non-linear behavior of stress around the fibers which produces regions of the matrix of high strain and high stress and regions of low strain and low stress. Nevertheless, in produces a good first approximation, and establishes a lower bound value.

Fibrous laminates are inherently anisotropic, so the engineering constants of the material, like the Young's modulus, shear modulus and Poisson's ratio are direction dependent. Some properties, like density and the longitudinal elastic constants, obtain good

predictions from this kind of approach, while others require more comprehensive models based on the theory of elasticity in order to obtain accurate predictions of the part's properties [17, 23]. For instance, this rule does not apply for the strength properties, since while the longitudinal Young's modulus is in general insensitive to the microstructure, the strength is highly sensitive to it (*e.g.* a polycrystalline's structure grain size affects the strength but not the modulus).

Since the Poisson's ratio for matrix and fiber are usually not very different, and it is often considered a secondary effect, the in-plane Poisson's ratio can be sufficiently predicted [24] by the rule of mixtures as:

$$\nu_{12} = \nu_f V_f + \nu_m V_m \tag{2.9}$$

The shear modulus (interlaminar and in-plane) can also be found by using the inverse rule of mixtures, in a similar fashion as the transverse modulus.

$$G_{12} = \frac{G_m}{1 - \sqrt{V_f}(1 - G_m/G_{f12})} \tag{2.10}$$

Having the effective properties of the composite, the analysis can be done on a macroscopic level, conducted for each lamina as a homogeneous material of said properties. Laminate composites are constituted by stacks of laminae. Each individual laminae may be oriented to obtain the necessary final properties required for the part, exploiting the inherent anisotropy of composites to tailor the material to suit the operation of the structure or part. After predicting or measuring the behavior of a lamina, a laminate can be approximated to the behavior of a stack of homogeneous orthotropic sheets with the effective properties estimated for the lamina [25]. This process can then be extended further, using the effective properties of each laminate (stack of lamina) to analyze large structures. This summarizes the concept of macromechanics: to establish the relationships between the laminae/their orientations and the final laminate properties (See Figure 2.3)

In the particular case of the conducted research for this work, matrix materials are considered isotropic and unidirectional bundles of fibers (the focus of this work) are considered transversely isotropic (same properties for any direction apart from along the fiber direction). Table 2.1 summarizes the elastic constants for a composite (Transversely isotropic). As the rule of mixtures is used to determine the homogenized properties of each lamina, the macromechanical analysis is done by means of finite element simulations.

TABLE 2.1: Summary of micromechanical calculations of the elastic constants for a transversely isotropic composite

Longitudinal Modulus	$E_{11} = E_{f1}V_f + E_mV_m$
Transverse Modulus	$E_{22} = E_{33} = \frac{E_m}{1-\sqrt{V_f}(1-E_m/E_f)}$
Shear Modulus (In-plane)	$G_{12} = G_{13} = \frac{G_m}{1-\sqrt{V_f}(1-G_m/G_{f12})}$
Shear Modulus (Interlaminar)	$G_{23} = \frac{G_m}{1-\sqrt{V_f}(1-G_m/G_{f23})}$
Poisson's ratio (In-plane)	$\nu_{12} = \nu_{13} = \nu_{f12}V_f + \nu_mV_m$
Poisson's ratio (Interlaminar)	$\nu_{23} = \frac{E_{22}}{2G_{23}} - 1$

2.4 Damage and defects in composites

Damage mechanisms in composites are often complex. There are several types which may be sustained during service, and defects which may appear during the manufacture. Their effects on the composite properties should be taken into account, and the conditions of failure should be known in order to guarantee safe and reliable use of the structure. Defects and failure are defined as follows.

Defect Material or structural flaw or damage. Unintentional local variation in the physical state or mechanical properties that may adversely affect the structural behavior of the component.

Failure When a material ceases to be able to perform its primary function adequately.

There are, in total, 52 reported defect types in composite structures [26], which can be grouped into specific categories. These may occur during material processing, component manufacture or in-service. Since the dimensions of the defect can have a bearing on how critical they are, defects are often characterized as microscopic or macroscopic, their criticality depending on shape, size, location, orientation and relative load-path, and frequency throughout the composite [27].

There are four main types of failure modes for composites. These are fiber failure, transverse matrix failure, interface failure and delaminations, distinguished by their macroscopic failure characteristics.

The standard damage progression in composites can be defined as multiple matrix cracking, scattered randomly throughout the material, followed by a stage of initiation of delaminations and localized damage at preferred weak spots such as ply interfaces, and finally by severe cracking and fiber failure [28].

CHAPTER 3

Sensors and techniques for Structural Health Monitoring and Non-Destructive Evaluation

Structural health monitoring and non-destructive testing both consist of many different techniques and make use of different kinds of sensors to monitor and interrogate the material in question. This section will focus on the sensors and techniques used and mentioned during the course of this work, specifically FBGs.

Namely, in the context of this work, the focus will be on fiber Bragg grating (FBG) sensors. Many applications have been reported for this kind of sensors, such as the monitoring of the resin cure of composites [7–9], in-situ measurements of strain and temperature [10–12], damage detection [13–15] and evaluation of patch repairs [16].

3.1 Optical Fiber Sensors

Optical fibers offer distinct advantages when compared to more common electrical sensors. Silica fibers are cheaper, less intrusive and lighter than copper wire due to the smaller dimensions, in addition to being immune to electromagnetic interference (EMI) and producing no heating through Joule effect [29]. These sensors can be classified by their structure, *i.e.* as intrinsic or extrinsic, by their change measured in the optical signal, *i.e.* intensity (*e.g.* microbending transducers), polarization (*i.e.* using Hi-Bi fibers), phase (*e.g.* Extrinsic Fabry-Pérot Interferometers) or wavelength (*e.g.* FBG), and by their implementation, *i.e.* as point, integrated, distributed or multiplexed. The fiber may be used solely as a means to relay the signal to and from an extrinsic sensor, located outside the fiber, or take the function of the sensing element as well for the case of an intrinsic sensor, where a section of the same fiber that carries the light input produces a change in the optical signal proportional to the measured parameters.

As such, a number of photonic sensors has been developed and studied for embedding. Some notable examples being extrinsic Fabry-Pérot interferometers [30], fiber Bragg gratings (FBG) [12] and distributed optical fiber sensors (DOFS) [31], among others, due to offering distinct advantages to other electronic analogous sensors (*e.g.* strain gauges), in the form of weight savings and less intrusiveness from embedding, especially when embedded parallel to the reinforcement orientation [2, 3].

This section introduces and discusses the basics of fiber optics. Furthermore, the optical sensors used for the execution of the experimental work are exposed and explained, as well as the applications, advantages and complications with regards to other commonly used transducers.

3.1.1 Optical fibers

An optical fiber consists of a cylindrical waveguide. Essentially, it is composed of a dielectric material, most often silica glass (SiO2). The fiber can be divided in three parts: the core, the cladding and the coating. The core and cladding are composed of the same material, but with different dopant concentrations, so the refractive index is not the same, granting the possibility of frustrated total internal reflection (FTIR), which is the principle which allows light to travel through the guide with minimal attenuation. The coating is usually a means of protecting the fiber and reducing its brittleness: Usually, it is either polyamide or acrylate. Acrylate coatings are cheaper and acceptable for most general cases, while polyamide coatings, as used in this work, are usually thinner (less intrusive when embedding due to the reduced diameter), withstand higher temperatures, and provide better adhesion to polymer matrices, being the most common choice for composite embedding in CFRP.

Besides SiO_2, other materials may be employed if the application requires it. For instance, sapphire glass has in the past been employed for very high temperature applications [32], and polymer fibers have been studied as a less brittle alternative to silica [33]. Two types of fibers should be distinguished: Multimode and single-mode. As the name implies, multimode fibers carry many modes of propagation of light, while single-mode or monomode optical fibers carry only a single mode.

3.1.2 Fundamentals

Light propagates inside a fiber optic as a dielectric waveguide. As an electromagnetic wave, the propagation and behavior can be fully understood, as with any medium, by a thorough examination of the Maxwell equations. For the purpose of the conducted

research, however, it is sufficient and instructive to consider a more simplistic model of light propagation inside of the optical fiber using ray theory. Afterwards, the wave nature of light is also consider in order to succinctly explain single-mode fibers.

Light rays traveling through a boundary of a refractive index change are refracted according to Snell's laws of refraction and reflection. It is possible, then, to define the maximum angle of incidence at the input face of the fiber that will propagate light. This is defined through the numerical aperture

$$NA = \frac{1}{n_0}\sqrt{n_{core}^2 - n_{cladding}^2} \tag{3.1}$$

which represents the sine of the maximum angle of incidence at the edge of the fiber, that results in light being propagated in the waveguide. n_0 corresponds to the refractive index of the medium that surrounds the fiber.

As such, an optical fiber's working principle revolves around having a higher refractive index in the core than the cladding, in order to contain the light inside of the waveguide through total internal reflection, and only light being reflected above this angle can be transmitted inside of the fiber.

3.1.2.1 Single mode fibers

Single mode fibers hold an advantage over multimode fibers by not experiencing mode dispersion: Different modes propagating have different effective indices and phase velocities inside the optical fiber, complicating the received optical signal, which in some applications is nothing but an optical disturbance. These fibers feature very small cores and very small index contrast, and as such the previously presented geometrical ray theory breaks down, as it ignores the wave nature of light.

A single mode fiber is that which carries only the fundamental mode , or LP_{01} (LP standing for linearly polarized) mode, which possesses an approximately gaussian intensity profile. Other modes are distinguished by the intensity profile of light inside of the fiber.

Consider a gaussian beam propagating through a homogeneous media. The beam will diverge as light advances further inside of the media (*i.e.* the edges of the wavefront will spread out as the light propagates). By having a different index in the periphery and center of the wavefront this effect can be mitigated, and light can be propagated inside an optical fiber. Therefore, in order to keep light inside of the waveguide, the optical fiber requires a core and a cladding.

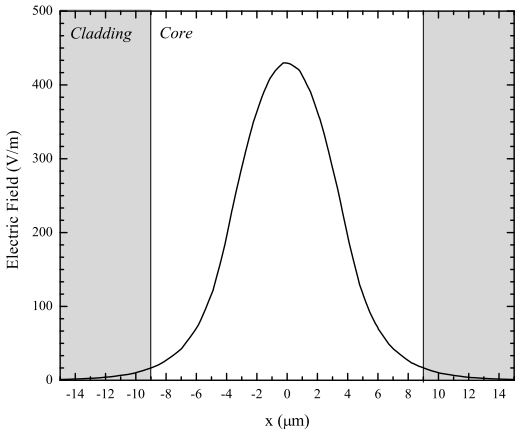

(A) Intensity versus radial position.

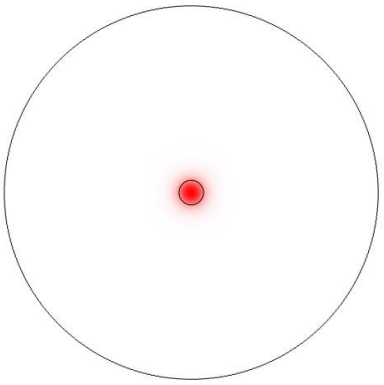

(B) Intensity distribution on the fiber and cladding.

FIGURE 3.1: Radial intensity profile of a single mode fibe for 9/125 μm fiber (Simulated in COMSOL Multiphysics).

In order to guarantee single-mode propagation, the refractive indices of core and cladding and the dimensions of the core must be considered. There are two very important parameters that define which modes propagate in step-index optical fibers, and also define the condition for single-mode guidance: These are the V number (also known as the generalized frequency), and the b constant (also known as the generalized guide index) [34].

$$V = \frac{2\pi}{\lambda} a \sqrt{n_{core}^2 - n_{cladding}^2} \tag{3.2}$$

$$b = \frac{n_{eff}^2 - n_{cladding}^2}{n_{core}^2 - n_{cladding}^2} \tag{3.3}$$

where λ is the vacuum wavelength of light and a is the radius of the fiber core and n_{eff} is the effective index for the propagated mode. These are usually plotted versus each other to draw the b-V diagram which can be used to easily determine which modes will propagate in an optical fiber and which will be in cut-off. Putting it simply, step-index fibers with a V value below 2.405 only propagate a single mode.

From 3.2, it is also insightful to realize that there is a wavelength threshold for the fiber to behave as a single mode:

$$\lambda_c = \frac{2\pi a}{2.405} NA \tag{3.4}$$

This is defined as the cutoff wavelength. Light with shorter wavelengths will excite more than one mode. From here, the core radius can be determined to the specified cut-off wavelength, in order to guarantee single mode propagation.

3.1.3 Fiber Bragg Grating

Fiber Bragg gratings(FBG) are intrinsic sensors which consist of a periodic perturbation of the refractive index in the fiber core. In effect, they work as a wavelength-selective reflection filter, or a stop-band filter in transmission. Their intrinsic capability to sense a multitude of measurands puts them a wide variety of mechanical sensing applications for different fields and industries: some examples are the monitoring of concrete bridges and domes, seismic activity, aerospace and wind-energy structural health monitoring. The gratings can be used for interferometric (phase) or wavelength sensor applications.

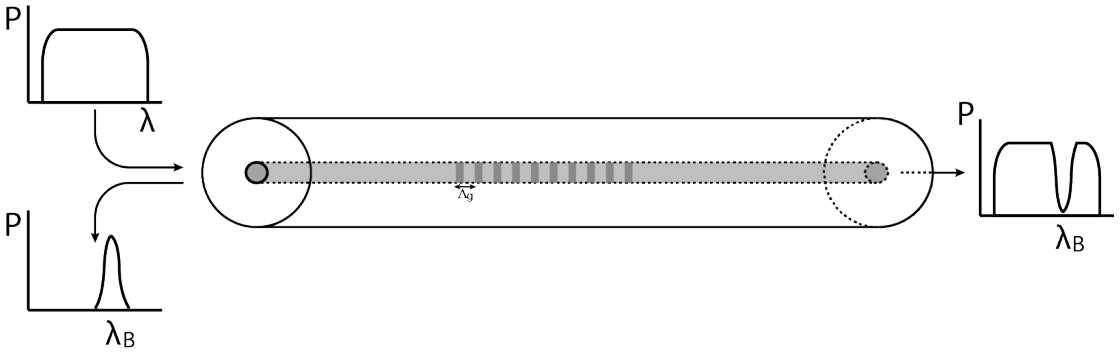

FIGURE 3.2: Representation of a fiber Bragg grating and it's spectral response in reflection and transmission.

Advantages of FBG sensorization stem from being a totally passive, small and low weight highly sensitive solution, with the ability to be read in transmission or reflection, requiring access to only one end of the fiber for interrogation, immune to electromagnetic interference, easily multiplexed and that can be used in harsh environments. FBG working on the C-band range (1525-1565 nm) are also suitable for remote applications due to the low attenuation of light in the optical fiber. FBG limitations involve their sensitivity to thermal disturbance or transverse strain (to a lesser extent), and the brittleness of the optical fibers.

3.1.3.1 Principle of work

A fiber Bragg grating (FBG) sensor consists of a periodic variation of the refractive index of an optical fiber. As light goes through a change in refractive index, part of the optical signal is transmitted and part is scattered. This will occur in the FBG at each index interface that exists in the grating. For one wavelength, all the successive reflections will be

phase-matched, interfering constructively, while the remaining spectrum will interfere destructively. By coupling the forward propagating core mode to the counterpropagating core mode under phase-matching conditions, the FBG will be appear transparent to the full spectrum, with the exception of a narrow band which will be strongly reflected around the Bragg wavelength, that is:

$$\lambda_B = 2n_{eff}\Lambda \tag{3.5}$$

n_{eff} being the effective modal refractive index and Λ the period of the grating. Essentially, the condition shows that the Bragg wavelength corresponds to light with a wavelength twice the period of the grating: The complex amplitudes corresponding to the reflected field contributions from different parts of the grating will all be in phase and interfere constructively. The magnitude of the index variation and length of the grating will determine its reflectivity [35, 36].

The use of FBG as sensors ultimately involves measuring the shift in the Bragg wavelength. The induced shift due to strain and temperature is defined as follows [36]

$$\lambda_B = 2n_{eff}\Lambda([1 - (\frac{n^2}{2} \cdot [\rho_{12} - \nu \cdot (\rho_{11} + \rho_{12})]] \cdot \Delta\varepsilon + [\alpha + (\frac{dn}{dT}) \cdot \frac{1}{n}]\Delta T) \tag{3.6}$$

$\rho_\alpha = (\frac{n^2}{2} \cdot [\rho_{12} - \nu \cdot (\rho_{11} + \rho_{12})$ being the photoelastic coefficient, with ρ_{ij} being the elements of the fiber optic strain tensor and ν being the Poisson's coefficient of the fiber, α being the coefficient of thermal expansion and $\xi = (\frac{dn}{dT}) \cdot \frac{1}{n}$ being the thermo-optic coefficient. For silica fibers with germania doped core, typical values are $\rho_\alpha = 0.22$, $\alpha = 0.55 \times 10^{-6}$ and $\xi = 8.3 \times 10^{-6}$ [37].

These occur due to index changes (due to temperature variation or deformation of the fiber, via photoelastic effects) and period changes (due to strain applied to the fiber or thermal expansion).

In silica fibers, the wavelength shift due to index changes are dominated by temperature variations and the period changes are dominated by the fiber deformation, the thermal expansion and photoelastic effects having a significantly lower impact [37].

Additionally, FBG sensors are sensitive to pressure changes (albeit with relatively low sensitivities), and can be made sensitive to other physical parameters by coating the fiber with materials that will convert the variation of such measurands into temperature or strain (*i.e.* coating with nickel to sense magnetic fields) [36].

3.1.3.2 Fabrication

The photosensitivity of optical fiber, and as such the ability to write permanent gratings in optical fibers were first demonstrated by Hill *et al.* in 1978, as a following to the research of the nonlinear properties of germanium-doped silica fibers. By launching visible argon ion laser radiation inside of a fiber, a incremental increase in reflection was noticed, as the standing wave intensity pattern created inside the fiber due to the forward propagating light and the back reflection at the end of the fiber increased the refractive index of the fiber and thus created a fiber grating (traditionally known as "Hill" grating). This technique is now commonly known as internal writing [35], and while it is historically relevent, the produced gratings were limited in application due to the working wavelengths, the production time and the inhomogeneities along the fiber [38].

Meltz *et al.* later reported on the holographic writing of gratings, by using two interfering beams external to the fiber, shifting the Bragg condition to specific useful wavelengths for telecommunications, which would be determined by the angle between the interfering beams (thus changing the grating's period) [39]. As opposed to Hill's method, this allowed the selection of Bragg wavelength by changing the geometry of the setup, instead of the incident light's wavelength. However, since the beams were travelling through free air, the setup had to be very well aligned: this method was prone to instability due to air turbulence or mechanical vibrations of the components, which could cause drifts in the formed fringe pattern (See figure 3.3) [40].

New and more reliable techniques for the inscribing of gratings in optical fibers were soon developed, such as the phase mask technique, introduced in 1993. This method still remains as one of the standards for grating manufacturing [41].

In addition, complex refractive index modulation and manufacturing techniques can be used to create other types of FBG, such as chirped, tilted, phase shifted and long period gratings (LPG) [42], or written in special kinds of fibers (*e.g.* High Birefringence) to achieve different spectral responses. One simple, but common and useful consideration in the modulation of refractive index during the manufacture of gratings is the gaussian apodization of the index, to suppress the appearance of side-lobes in the reflected peak, which can be useful for wavelength-division multiplexing (WDM) applications. Erdogan [43] did an extensive study on the spectral properties of different grating designs and with varying apodization.

Currently, the most common approach for manufacturing FBGs is the phase mask technique. Other, more recent methods have been developed, such as point-by-point writing [44], which consists in focusing a laser (UV or infrared intense ultrafast pulses) pulse

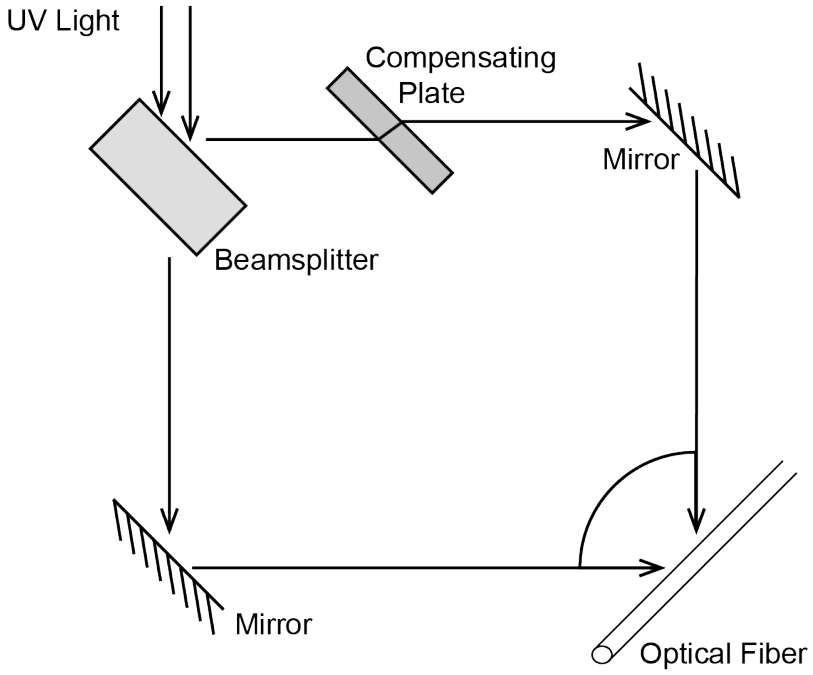

FIGURE 3.3: Example of Meltz's holographic set-up for imprinting FBG sensors by creating a laser interference pattern.

in an optical fiber. It has shown relevance particulary in the design of LPG gratings, where the positional accuracy is not as demanding. It produces the advantage of not being limited to one grating period by the phase mask, and by not requiring the doping of the fiber to increase photosensitivity, by working through non-linear effects (two-photon absorption) at the region of focus of the incident beam.

Phase Mask

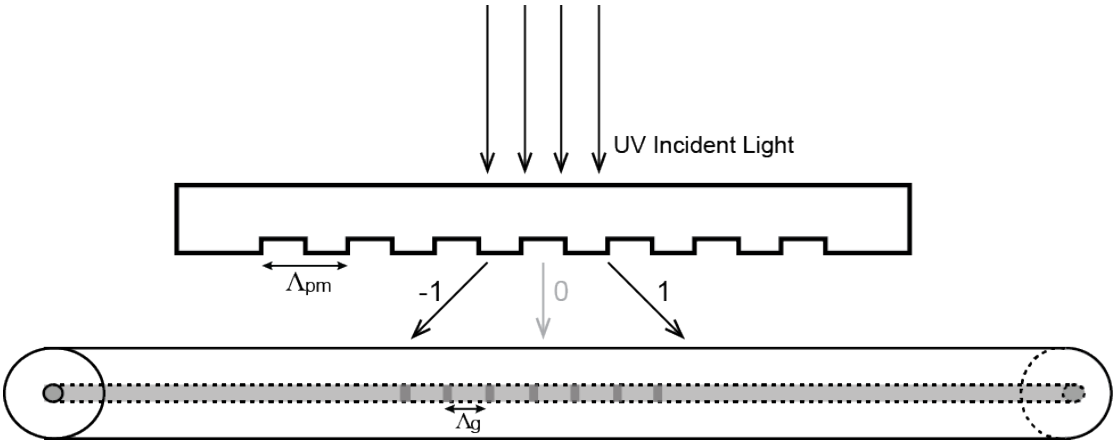

FIGURE 3.4: Phase mask technique and diffraction orders represented. Note that the zeroth order is suppressed.

This is the most commonly used technique for manufacturing FBGs. A phase mask is made by etching a relief grating in a silica plate (transparent to ultraviolet light), with the purpose to create a diffraction pattern from an incident ultraviolet (UV) light source, thus replacing the need for the interferometer. Ultraviolet light incident normal to the phase mask is then diffracted by the periodic corrugations.

By requiring lower stability apparatus and lower laser coherence, this technique carries the advantage of greatly simplifying the manufacturing process, while yielding gratings with a high performance using cheaper laser sources. Furthermore, it allows the manufacture of several gratings at once using the same phase mask. It is also easy to introduce apodization functions to suppress sidelobes using this technique, and it has been extended to the fabrication of special kinds of gratings.

As the laser light beam meets the phase mask, it will be diffracted into several orders of diffraction. Most of the diffracted light is contained in the 0, +1 and -1 orders [35]. The +1 and -1 orders produce the periodic pattern, which can be used to hit the photosensitive fiber and inscribe the grating. In general, the intensity of the +1 and -1 order must be equal in order to efficiently inscribe the grating, and the 0 order should be minimized. For that, the phase mask is designed to suppress or minimize the zeroth order (transmitted beam), by controlling the depth of the corrugations.

The laser wavelength does not alter the grating period, being therefore selected to correspond to the absorption band of germanium glass defects, so the photosensitivity may be easily increased by germanium doping or hydrogen loading. The imprinted grating's period (Λ_g) is then defined independently of the incident light wavelength, by the period of the relief grating etched in the phase mask (Λ_{pm}), as

$$\Lambda_g = \frac{N\lambda_B}{2n_{eff}} = \frac{\Lambda_{pm}}{2} \tag{3.7}$$

where $N >= 1$ is an integer indicating the order of the grating.

However, the incident wavelength remains relevant for the suppression of the zeroth order, as the corrugation depth is a function of the wavelength and optical dispersion of the material of the phase mask.

Phase masks can be used with light normal and non-normal inciding light. Non-normal incidence requires suppression of higher diffraction orders to equalize the intensity, so in general, it is more cost-effective to use the phase mask at normal incidence [45].

3.1.3.3 Multiplexing and interrogation

One of the most promising aspects of optical fiber sensors is the capacity for multiplexing and accessing multiple sensors in a single fiber: Many applications of FBGs, namely structural health monitoring or non-destructive testing, want to measure as many points in line as possible preferably using the same fiber, in order to maximize the points of interrogation, minimize the influence in the surrounding local properties and minimize overall costs. In order to achieve this, it is important to understand how one can multiplex the optical signal from several in-series FBG. The two most common ways of multiplexing FBGs are Wavelength Division Multiplexing (WDM) and Time Division Multiplexing (TDM). Often, for optimal results and maximization of the number of multiplexed sensors, both techniques are used simultaneously.

The wavelength encoded nature of a Fiber Bragg Grating facilitates WDM. By allocating each of the multiplexed sensors a different slice of the spectrum, using different Bragg wavelengths for each of the FBGs, analysis of the reflected or transmitted spectrum allows us to track the several peaks and infer the shift of each individual sensor. This method is limited by the operational bandwidth of each sensor and the expected shifts of each grating (two consecutive peaks become indistinguishable if they ever overlap), and by the light source profile width [37]. WDM interrogation systems are typically high in sensitivity and accuracy, with moderate measuring frequency [46].

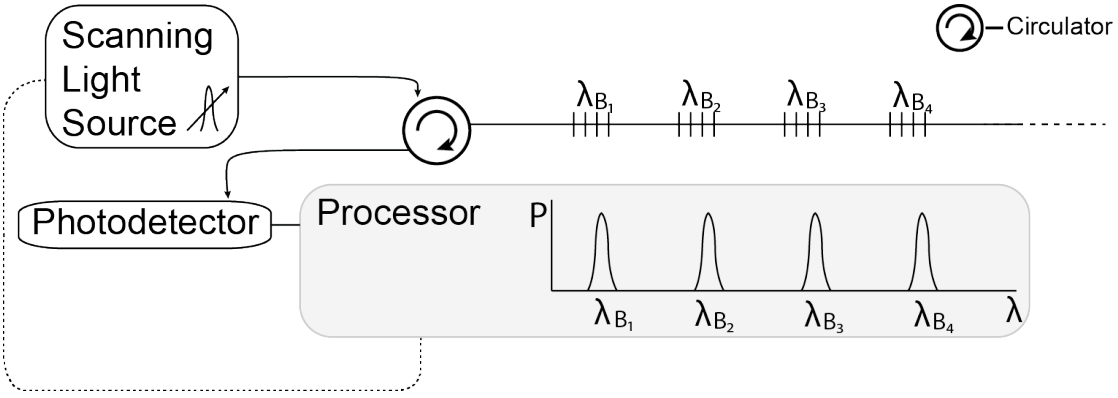

FIGURE 3.5: Wavelength division multiplexing interrogation system example.

TDM involves sending a pulsed light signal, into a fiber and discriminating the reflection from each sensor by selecting the corresponding time window to the sensor to be interrogated. The light will have to travel a greater path for each subsequent FBG, and as such, the reflection of each FBG will arrive at different times. The optical signal time of flight can be determined by the distance light travels inside the fiber, the effective refractive index of the media and the speed of light.

$$T_{round-trip} = 2 \cdot d \cdot (\frac{c}{n_{eff}}) \tag{3.8}$$

c being the speed of light in a vacuum, n_{eff} the refractive index of the medium and d the distance from the system to the sensor.

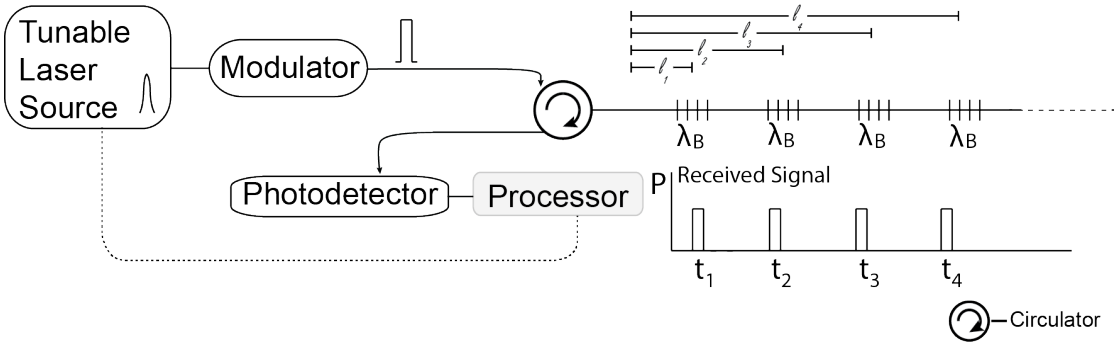

FIGURE 3.6: Time division multiplexing interrogation system example.

A TDM system can be designed in some different possible configurations, such as using a series of low reflectivity FBGs in order to allow the transmission of light in both ways of the optical path, all with the same Bragg wavelength. The maximum number of FBGs multiplexed by TDM is limited by the reflected power of the last multiplexed sensor, as this will produce the most attenuated signal and it should be sufficiently higher than the noise floor in order to allow for relevant measurement. Besides the noise, TDM may also measure some interference effects: Assuming all sensors to be spaced equally, each N_{th} sensor will have (N-1) interference contributions to the signal due to multiple back-and-forth reflections which arrive simultaneously (due to the same length of the optical path). This interference can be minimized by keeping the FBG reflectivity low. These systems often posses high measuring frequency and robustness, but have restricted multiplexing capability and require relatively large spacing of the sensors to achieve adequate time differences.

By combining WDM and TDM, one can multiply the number of sensors per fiber by reusing the full spectrum of the source. Launching a pulse of light from the source, the reflections from FBG's at successively more distant positions along the fiber will return to the detector at successively later times (TDM). One can then multiplex clusters of WDM multiplexed sensors, and access each of the clusters by selecting the appropriate time window to interrogate.

By selecting only a certain window of time to be analysed, only a single WDM set of sensors is selected for interrogation[37]. The only additional requirement is that the modulated pulse has to be wide enough to cover the whole WDM multiplexed cluster.

Afterwards, any time window correspondent to each of the clusters may be selected for interrogation via TDM.

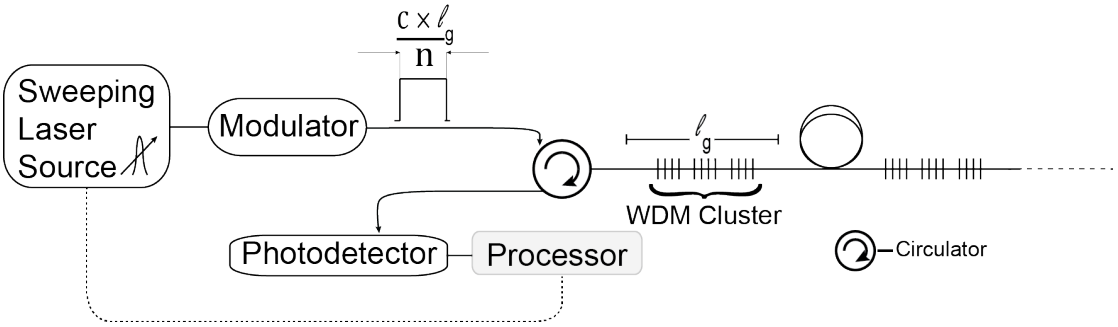

FIGURE 3.7: Example of a simultaneous TDM and WDM interrogation system.

CHAPTER 4

Smart composites: Considerations, techniques and state-of-the-art

"Smart materials" are materials whose properties react to changes in the environment, either by responding to them through actuators or by reporting their status to a technician or operator. Along with the obvious increase in the safety margin and efficiency of these materials with respect to their regular counterparts, they may offer greater cost efficiency in the long run due to more accurate assessment of the material's state and better production yields.

One common way of achieving smart materials is by embedding sensors and actuators, in a way that produces minimal influence in the host structure's properties. Hereupon, the composite becomes able to sense its own state for the non-destructive evaluation of the manufacture procedure and final part, the monitoring of in-situ operation and for detection of damage.

To achieve this end, several types of sensors can be employed. One increasingly popular method, which is the focus of this work, is through embedded optical fibers. Over the course of this work, embedded FBGs are tested for applications in monitoring of the manufacture of composite plates, monitoring of the operation in real time and detection of damage.

4.1 Embedding considerations of sensors on smart structures

Embedding the sensors (namely optical fibers) offers the possibility of local monitoring while protecting the sensor. However, the embedding process in composite materials raises some challenges and demands careful planning and considerations prior to the lay-up of the part's preform. Specifically, it is important to assess how to access the

sensors, where to ingress/egress them from and how to protect those regions, how to fix them in the desired place during the whole process, and how to protect the connectors/fibers/wires during the manufacture, all the while considering the embedding and sensor's influence in the local material properties and attempting to minimize it. In the case of cure monitoring, there's also the need to determine how to access the connectors while the part is enclosed in a curing oven, autoclave or vacuum plate.

Owing to the fact that composites are made of a wide range of combinations of materials, each specific fabrication technique delivers unique challenges to the integration and ingress/egress of the optical fiber. In general, care must be taken for the fiber/coating to not interact chemically with the host material during fabrication: both must be able to withstand the high temperatures, and preferably have thermal expansion coefficient similar to the matrix.

As a foreign entity to the structure, embedded sensors invariably introduce a local change in properties [47], while also fostering the creation of resin pockets around the optical fiber [48] which further induce stress concentrations that may degrade performance and durability. The influence will ultimately depend on the optical fiber dimensions, its coating, relative orientation to the reinforcement and type/direction of load (*i.e.* fatigue, quasi-static, impact) experienced by the material. Previous studies [49] show that the stiffness, strength and Poisson's ratio are not significantly affected by the embedding of optical fibers under quasi-static tensile loads, and neither is the matrix cracking behavior. However there's some reduction in the fatigue life of the composite plate correlating to the amount of embedded optical fibers. Benchekchou *et al.* [50] also studied the fatigue behavior of composites with embedded optical fibers and concluded that fatigue may eventually lead to delamination and debonding of the fiber due to the stress formed at the interface between coating and specimen, and that the location of the sensor on the plate is important to the ultimate fatigue response.

Complementary, Roberts *et al.* [51] studied the effects of embedded optical fibers in longitudinal and transverse tension, longitudinal compression and shear, finding that embedded polyimide coated fibers have suitable properties to embed in reinforced thermosets. His group verified that it is possible to choose host materials that generally do not have their static (or quasi-static) mechanical properties degraded by the embedded sensors, although some samples saw a decrease in longitudinal compressive strength. Furthermore, some indication that fibers aligned with the reinforcement and load pose less influence in the ultimate material properties than transversely aligned ones was also observed. This topic was further developed by Shivakumar *et al.* [2], by studying the influence of optical fibers embedded at different angles relative to the reinforcement,

in tension and compression, and varying the laminate thickness. Although the modulus remained generally unaffected, the tensile strength reduced 0-5% and compressive strength reduced from 10 to 40%, depending on the orientation of the embedded fibers. Orienting the fibers perpendicularly to the reinforcement once again showed the most severe effects. The authors concluded that the reason for the decrease are matrix pockets and greater misalignement of the reinforcement due to the presence of the fibers, measuring the resin pocket area to be up to 10 times greater than that of the optical fiber. The geometry and effects of resin pockets, and the deformation field caused by them, had been studied by research groups such as Melin *et al.* [52], measuring the deformation fields around optical fibers during transverse loading using Moiré interferometry (by measuring changes in the reflection pattern from the laminate), and comparing the experimental results to a numerical FE analysis, showing that the strain fields inside the composite are changed around the optical fiber, with the effect being dramatically reduced with the distance from the fiber.

Besides the loading type and fiber orientation, it has been shown that the fiber coating plays a pivotal role in the embedding influence to the surrounding properties and sensor measurements. The coating needs to be chemically compatible with the matrix to ensure a good interface and prevent slippage, which is crucial for the sensor's ability to measure strain and guarantees the least influence in a material's local mechanical properties [53]. The coating influence on the embedded sensor's performance and mechanics was studied by Dasgupta *et al.* [54] and Sirkis *et al.* [55], presenting even analytical evidence of the existence of optimal coating material/thickness combinations for a given host material, minimizing or even eliminating stress concentrations in the specimen, optical fiber and the coating itself.

In addition to the deliberations on the mechanical influence of embedding, the methods and techniques for embedding must also be discussed, such as how to best access the embedded fiber. Reflective measurements have the obvious advantage of requiring a single access point to the fiber, while transmission measurements always require access to both ends for input and output of light. There are two possible solutions for the fiber to exit the material: either the fiber exits through one of the composite edges, or it rises through successive plies and exits perpendicular to the plane. The former method has the distinct advantage of producing the least influence in the material's properties, but it limits any ensuing machining of the material as it will break the fibers, without any chance of subsequent splicing. The latter leaves the edges free to cut and tailor the part's final shape, but produces the greatest influence in the mechanical properties of the composite [56]. Finally, the egress/ingress region should be protected to prevent breaking of the fibers during debagging or operation. Often, PTFE (Teflon) or metallic tubes are used to protect the entry spot.

Periodic reevaluation of the sensor may be required, as over time, not only the material may fail or degrade, but also the sensors. Optical fibers should hold loads much greater than the failure loads of the host material without sustaining permanent damage or significant alterations to their response [47]. Dong Gun Lee *et al.* [57] studied the durability and resilience of embedded fiber optic sensors, reporting evidence that extrinsic Fabry-Pérot Interferometric (EFPI) strain sensors should survive during the typical life of aerospace structures for quasi-static and tension-tension fatigue loads.

4.2 Manufacture Monitoring

The composite manufacture processes and their control have seen some advances with the improving of technology and infrastructure required to enable the automation of setting specific parameters and their rate of change at predefined times, during a specific cure cycle, such as heat and temperature or pressure.

Composites, however, present complex and often unpredictable behavior during the cure: the curing rate may vary from part to part due to the age of prepreg and resin, environmental conditions during the lay-up of the preform, different conditions of the mold and tools used, uneven temperature profile inside the part during curing, among other causes, which may alter the cure response and end up affecting the final properties of the part. Likewise, during the cure void-heavy sections of the part, uncured regions, or residual strains may develop which ultimately lead to strength reduction, cracks and delaminations. In order to prevent undercured parts with suboptimal properties or brittle overcured parts, composites are often built within a safety margin.

With this in mind, monitoring the manufacture may hold the solution to optimize yields and improve the consistency in the produced composite structures. Embedded sensors can measure the variations to the material during the cure, enabling the determination of each part's optimal cure endpoint, tailor cure schedules to suit the resin age and chemical integrity and offer quantitative feedback on the cure process.

The inspection of the resulting part itself can easily be done by destructive methods or other analytical instruments like rheometers, or other techniques such as differential scanning calorimetry, infrared spectroscopy, nuclear magnetic resonance, gel permeation chromatography, among others. These, however are not very useful as they cannot readily be applied to in-situ industrial cure monitoring in many cases, and the expensive equipments often works only with samples of small dimensions. For industrial purposes, dielectric, acoustic, ultrasonic, thermal and optical fiber methods have been reported. Several of these techniques were thoroughly compiled and reviewed by Schubel *et al.*

[58]. Optical fibers show promise due to not being overly intrusive to the material properties, and have been extensively used in the past in the form of EFPIs, FBGs, and other sensor types [59–61]. There are essentially two reported methods for cure monitoring using optical fibers: Strain measurements (*e.g.* using FBG or Fabry-Pérot sensors) or measurement of the Fresnel's reflection intensity at the end of the fiber (the refractive index of the resin changes as it cures) [62]. The case of strain measurement through optical fibers is especially relevant, since there's also the added advantages of easy multiplexing, residual strain information, and posterior harnessing of the same sensors to monitor the local state of the structure in-situ and during real-time operation.

During vacuum assisted resin infusion techniques (the fabrication method of choice for the conducted work), the mould and fabrics are sealed by a vacuum bag film and tacky tape, as to compress the preform and achieve a high fiber volume fraction, and to create a differential pressure to force the resin to flow and infuse the fabrics from the inlet to the vacuum outlet. For optimum manufacturing, it is essential to monitor the process to prevent defects such as dry spots and uncured regions, and to get a real-time assessment of the cure [63]. In addition, it enables the study and calibration of the correct temperature profiles, when the temperature may not be uniform around the composite plate (*e.g.* when the cure is performed in heated vacuum table, as opposed to a curing oven), giving also information on the temperature profile inside the composite (which will not be uniform through thickness) and how these parameters ultimately affect the cure. Also, it may be able to identify vacuum failures during the cure, which may have occurred due to improper manufacture of the preform and bag, resin blocks or some other malfunction [64].

Besides the optimization of processes and detection of malfunctions, monitoring by means of embedded sensors can enable study of the glass transition and of the residual strains existing in the composite after manufacture. These residual stresses and strains are self-equilibrated, supported by a body in the absence of external loads, and play an important role in the mechanical performance of the final part. The formation of residual strains during cure can occur due to the glass transition or polymerization of the resin, the elevated temperatures due to exothermic reactions, the shrinking of the resin coupled with the mismatch between the elastic and thermal properties, the behavior during the cure between the matrix and reinforcement [65] and interactions of the part and mould [66, 67].

These induced residual strains can later lead to warpage and spring-back, complicating the part's use in the assembly of structures, in addition to having effects in the end properties of the product [68]. Hyun-Kyu Kang *et al.* observed the warpage due to residual strain formation using a sensor head comprised of a FBG/Fabry-Pérot pair, and studied

the residual stresses in two orthogonal directions for unidirectional, bidirectional and asymmetrical laminates [69]. Warping is commonly verified in composites with assymetrical lay ups due to the imbalance in the stresses created during the cure of the resin. Zhan-Sheng Guo *et al.* [70] proposed that the warping can be studied by measuring the residual strains using embedded FBG sensors in asymmetric cross-ply laminates, and confirmed observing the resulting shape of the resulting part (which agreed the FBG predictions).

Early monitoring studies involving fiber optic extrinsic Fabry-Pérot interferometric by Lawrence *et al.* [59] measured the residual strain formation during the cure non-destructively. Chen *et al.* [60] monitored the cure using the same kind of embedded sensors, and compared the results to an ultrasonic sensor, for complementary monitoring. Finally, they compared the degree of cure to that measured using a destructive analysis by differential scanning calorimetry (DSC).

Leng *et al.* [71] studied and compared the viability of embedding FBG and extrinsic Fabry-Pérot interferometers (EFPI) sensors to monitor the cure process, detecting the vitrification of the epoxy and measure the residual strains, getting good correlation for the results measured by both sensor types. Later, they used a similar setup to compare the cure and posterior response to a three-point bending test of composites with and without defects [72]. Similar experiments using FBG only were performed by Murukeshan *et al.* [73], with an emphasis on composite response to bending tests performed after the cure monitoring. FBGs were also used to monitor the residual strain formation by Parlevliet *et al.*, while also measuring thermal gradients through the thickness as a potential precursor to the residual strain formation [74]. The measured variation in peak temperatures could be related to the thermal residual strain levels. The glass transition was also observed. They concluded that the residual strain gradient most likely appears due to thermal shrinking of the composite, although they lacked a temperature reference for the FBG. The attempt to optimize of a cure regime was done by Harsch *et al.* [75] by monitoring of the final residual strains and trial of different cycles and incrementally tuning the parameters. Aktas *et al.* [63] used FBG sensors to monitor the cure of novel matrix blends, using long and complex curing cycles (24h), successfully using a temperature reference FBG.

FBG sensors were also used to measure the residual strains and their redistribution in the vicinity of a longitudinal crack by Colpo *et al.* [76], and de Oliveira *et al.* [67] measured the influence of the mould thermal expansion in the development of residual stresses in the composite using fiber Bragg gratings, for unidirectional and crossply laminates using different moulds. This was further developed by Khoun *et al.* [66], who also used FBG sensors to monitor the in-plane strains developed during a resin transfer

moulding manufacturing process, observing the formation of residual stresses during the sample cooldown resulting from the thermal expansion coefficient mismatch and polymerization of the epoxy. They captured in the FBG the separation of the laminate from the mould, and compared the FBG results with predictive FE models, to determine the tool-part interactions.

In addition, FBGs were used to characterize the thermal expansion and residual strains in cylindrical specimens by Karalekas *et al.* [65], by using long FBGs to evaluate the strain along the FBG, without influence from resulting spectral distortion, supporting the data with numerical modeling. The effect of the manufacture on the final grating's spectrum after embedding in advanced composite materials and fiber/metal laminates, was reported by Kuang *et al.* [77].

This work focuses on the monitoring of unidirectional and bidirectional sections of the material, the study of the effect of the manufacture on the ultimate sensor's response and the observation of the local residual strains of the composite.

4.3 In-situ real time monitoring

Embedded sensors can create smart structures able to monitor their current state. Specifically, two relevant physical parameters to monitor are the real-time local deformation of the part and its temperature. Ultimately, deformation measurements determine the tensile or compressive strain state of the part or its curvature (which may be indicative of imminent failure), characterize oscillations or vibrations and detect load/overloading which can be addressed promptly either via actuators or by timely reporting of the material state to a competent operator. Also, sensors close to damage may perceive local changes in sensor spectral response [78], as was shown by Epaarachchi *et al.* with near-infrared Bragg gratings, and correlate that with local damage accumulation. Local temperature monitoring may also be relevant for applications where the thermal state of the material is important for its operation, or where it might be interesting to study the temperature profile and how it propagates while the structure is in operation. Additionally, local measurements allow the comparison and validation of simulated finite elements model which can prove helpful to predict the material's behavior in each situation.

Composites, in particular, due to their difficulty for repair, and degradation of strength with time and the complex damage and failure mechanisms require close monitoring to prevent unexpected failure [79], and their layered structure offers additional challenge with predictions by recurring only to surface sensors. Fiber Bragg gratings have been

extensively studied and show promising results as embedded sensors for composite materials and structures [5] due to their ease in multiplexing and cost efficiency [6]. Davies *et al.* [80] shows their applications to fast and reliable monitoring naval applications by installing FBGs in a 35m carbon fiber yacht mast, for both short-term and long-term testing, monitoring real time strains in the material and using defined baselines to determine the condition of the surrounding material through future comparison, and attesting the viability of these kinds of sensors for marine applications, while Kahandawa *et al.* [79] assessed the embedding and viability of FBG sensors for SHM applications in aerospace structures, measured the resulting distortion of the FBG peak during curing, torsion and microbending of the fiber, and studied possible causes for the distortion. Furthermore, the study concluded with an attempt to relate the distorted spectra with damage.

In-situ measurements of strain and temperature [10–12] are a recurring focal point of many studies, as the cross-sensitivity of both parameters often presents a challenge that must be overcome for the design of new sensor heads. As such, when the sensors are to be used in operation environments without controlled temperature, some form of thermal compensation has to be applied. In the past, simultaneous measurement of temperature and strain with FBGs has been shown by using special kinds of FBG. For instance, Patrick *et al.* used a combination of FBGs and LPG and measuring the reflected signal, evaluating the LPG wavelength shift through its influence in the reflection intensities of two FBGs [81]; James *et al.* [82] used two different diameter fibers spliced, each with an FBG, to discriminate the response. The setup, however, proved exceptionally weak at the splice joint; Guan *et al.* designed a sensor head consisting of a superstructured FBG to measure both parameters simultaneously with the transmitted signal wavelength and intensity [83] and another using a single FBG imprinted on a splice joint between two fibers producing two Bragg wavelengths and two different temperature sensitivities [84]; Peng *et al.* solved the issue by employing low-reflectivity FBG sensors and using Raman scattering as a temperature reference by analyzing the measured stokes and anti-stokes shift, doing a pulsed wavelength-sweep to interrogate the FBGs and fixing the wavelength outside of the FBG range for the Raman interrogation [85]; Hi-bi fibers were used by W. Urbanczyk *et al.*, by using a bow-tie birefrigent fiber with an imprinted FBG, essentially dividing the reflected Bragg wavelength in two peaks and measuring their separation as a temperature reference in addition to the shift [86], by M. Sudo *et al.* using hi-bi PANDA fibers [87] and L.A. Ferreira *et al.* using similar bow-tie fibers to achieve simultaneous measurement with interferometric interrogation of the reflected wavelenghts by the light polarized in the slow and fast axes [88]; Wei-Chong Du *et al.* [89] designed a fiber grating Fabry-Perot cavity (GFPC) composed of two FBGs possessing two spectral peaks within the main reflection band with the normalized power difference changing linearly with temperature and strain, in addition to the wavelength

shift; and Jaehoon Jung *et al.* used erbium-doped [90] and erbium:ytterbium-doped [91] fibers' as a temperature reference by measuring the linear variation in the spontaneous emission power.

While all the aforementioned solutions are interesting and potentially relevant, most are not suitable for structural health monitoring applications where reliability, cost-efficiency and simplicity of the interrogation setup are crucial. For that specific purpose, several techniques have also been considered: The simplest cases are to use one of the gratings as a temperature reference by making it strain independent (by means of a capillary) [92, 93] or to use two FBGs (not multiplexed) with vastly different Bragg wavelengths, requiring two different light sources. Other proposed answers consist in embedding a pair of FBGs and employing the local properties of the composite material surrounding the sensors to solve the temperature compensation issue. In this context, the local response to strain and/or temperature of a sensor has been shown to change by means of employing different numbers of lamina and varying the local composite thickness around each FBG by O. Frazão *et al.* [94], or by using different surrounding matrix types for each FBG of the pair by M. S. Ferreira et al [95]. Likewise, L. Rodriguez-Cobo *et al.* demonstrated the same effect by varying the width and geometries of composite plates, and by inducing damage close to one of the sensors (and even using a single long FBG) and thus altering its strain response [12].

Supplementary to strain monitoring, the aforementioned methods can also be adapted to monitor applied load on structures. This, of course, is just a matter of using the right coefficients to convert wavelength measurements into load, or having the correct material properties and coefficients to convert strain into load (assuming elastic behavior), which may have limited, but instructive applications.

The conducted work in the context of this dissertation fits the context of local alteration of the material properties, by embedding a pair of FBGs in a composite with two sections made of different ply stacks.

4.4 Damage detection

When compared to using the sensors to detect existing damage and defects or their formation, it is relatively simple to directly sense measurands like strain and temperature, as presented before. Damage assessment poses extra layers of challenge in the form of the interpretation of the various kinds of damage and damage mechanisms in CFRP, which, to further complicate, may not appear in isolation. Also, this kind of detection requires analysis of the effect of each of the stimuli on the sensor output, which may not

be easily predicted, and the techniques for the interrogation of the material in general are not as straightforward.

One such technique is that of ultrasonic guided wave propagation inside the material, to sense existing damage and defects in the composite by detection of the acoustic interfaces present in the material. Another related example is that of acoustic emission, which uses a similar setup, but only listens to acoustic events by the material itself, producing a passive interrogation of the formation and propagation of damage.

4.4.1 Acoustic sensing

Acoustic waves can be propagated through the material by actively placing some sort of actuator (such as a piezoelectric or magnetostrictive material) in contact with the material and producing a vibration (Commonly known as guided Lamb waves). Sensors can be bonded to the material in order to sense the acoustic events produced on it, as a result of impacts, damage formation or propagation. Discovered by Horace Lamb in 1917 and introduced as a means of damage detection by Worlton *et al.* [96] in 1961, Lamb waves have established their position as prominent non-destructive evaluation tool.

The advantages featured by this kind of inspection involve the ability to inspect large structures while retaining their coatings and insulation, the ability to inspect the entire cross section, lack of need for expensive devices to handle and manipulate the part during inspection, excellent sensitivity to multiple defect types (Potential damage types to be identified via Lamb wave inspection have been summarized by J.L. Rose [97]), low energy consumption and great cost efficiency [98]. This technique enables several types of studies on the material, from qualitative studies which are indicative of damage, to a quantitative assessment of its position and estimation of its severity, both of which can be used to a prediction of the remaining service life, as shown by Worden *et al.* [99]. The limitations come from the complexity of the propagation of these waves in non-homogeneous and anisotropic media. Waves reflected from the material boundaries may complicate the signal processing, the analysis of the obtained results and even conceal possible damages.

New fiber-optic acoustic sensor alternatives for the aforementioned purposes have been studied and shown the ability to compete or complement the more standardized and established piezoelectric transducers.

4.4.1.1 Principles of guided Lamb wave emission

Lamb waves consist of a superposition of longitudinal and shear modes. Several modes may be excited through the material, which in general can be divided in symmetric and anti-symmetric, and an additional mode - shear horizontal (or love wave) perpendicular to the wave travel has also been confirmed by finite element simulation and experimental studies [100, 101]. The first two are the modes relevant for damage detection. The conditions for the propagation of each are as follows [102]:

$$\begin{array}{rcll} \frac{\tan qh}{\tan ph} & = & -\frac{(4k^2qp)}{(k^2-q^2)^2}, & \text{symmetric} \\ \frac{\tan qh}{\tan ph} & = & -\frac{(k^2-q^2)^2}{(4k^2qp)}, & \text{anti-symmetric} \end{array} \tag{4.1}$$

$$p^2 = \frac{w^2}{c_L^2-k^2}, \quad q^2 = \frac{w^2}{c_T^2-k^2} \quad \text{and} \quad k = \frac{w}{c_p} \tag{4.2}$$

h being the plate thickness, k the wavenumber, c_L and c_T the velocities of transverse and longitudinal modes, c_p the phase velocity and w its frequency.

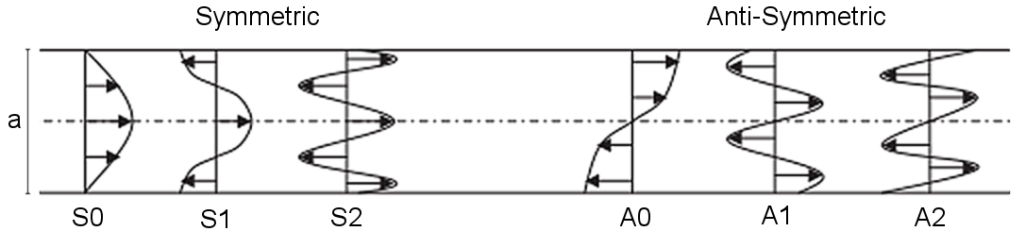

FIGURE 4.1: Depiction of symmetric and anti-symmetric wavefronts through a plate of thickness a. (Adapted from [103]).

From the equations, it is notable that regardless of mode, the Lamb wave velocity is dependent of frequency, and as such they experience dispersion, which varies from mode to mode. The mode propagation is also different at each frequency and their susceptibility to types of damage varies, the understanding of which is pivotal for effective application of the technique. Dispersion, being the phase velocity change with regards to the input frequency, can be controlled by using an excitation of a more defined frequency. The trade-off for having a better defined excitation frequency is that of less time definition: Guided Lamb waves are produced by sending a short tone bursts through the material. In order to prevent heavy dispersion effects, a windowed burst in usually applied, as opposed to a single pulse. The envelope function of the sent burst is computed via the Hilbert transform and then the group velocity can be defined through computation of the time of flight from the maximum of the envelope to that of the received wave packet.

The selectable frequency range for a Hanning windowed toneburst of cycle number n and frequency f_0 is defined as

$$\frac{f_{min}}{f_{max}} = f_0(1 \pm \frac{k}{n}) \tag{4.3}$$

k being a constant dependent on the definition of bandwidth. As presented, the frequency accuracy, and as such the dispersion effects are reduced by increasing the number of cycles in the burst [104]. The compromise comes from the increased the number of cycles increasing the $T_{initial}$ (Duration of the sent burst), but decreasing the T_{disp} (the duration increase of $T_{initial}$ as a result of dispersion over a given distance). Having higher $T_{initial}$ compromises the time definition, since long signals may create overlap between incident and reflected waves [104].

Depending on the application, 3 or 5-count bursts are often used. Another approach to determine the most suitable cycle number and frequency for a Lamb mode is the minimum resolvable distance approach [105].

$$MRD = \frac{v_0}{d}[l(\frac{1}{v_{min}} - \frac{1}{v_{max}}) + T_{initial}] \tag{4.4}$$

where l and d are the wave propagation distance and plate thickness, v_0, v_{min} and v_{max} are the phase velocities of the central and minimum and maximum frequencies in the wave packet, and $T_{initial}$ is the duration of the sent wave-packet. The MRD is essentially the distance covered by the center frequency in the time corresponding to the duration of the received waveform (broadened through dispersion), divided by the thickness of the composite plate. The smaller a MRD value, the better the resolution. A0 and S0 modes are usually observed to possess very low MRD values, and as such they are often the excited modes for damage detection. A0 is observed to be more sensitive to surface defects (*e.g.* cracks or corrosion), while S0 remains reasonably sensitive throughout the thickness. In general, analytical models for Lamb waves are very complex and studies often turn to numerical simulations [102].

4.4.1.2 Lamb wave emitters, transducers and techniques

Lamb waves sent through the material will propagate, and can be received by other transducers placed throughout the material. Guided waves often involve getting a reference baseline measure for the structure before it goes in operation in order to compare to future measurements during operation, and detect any defects that will cause alterations to the propagated wave. Although this does not determine the nature of the

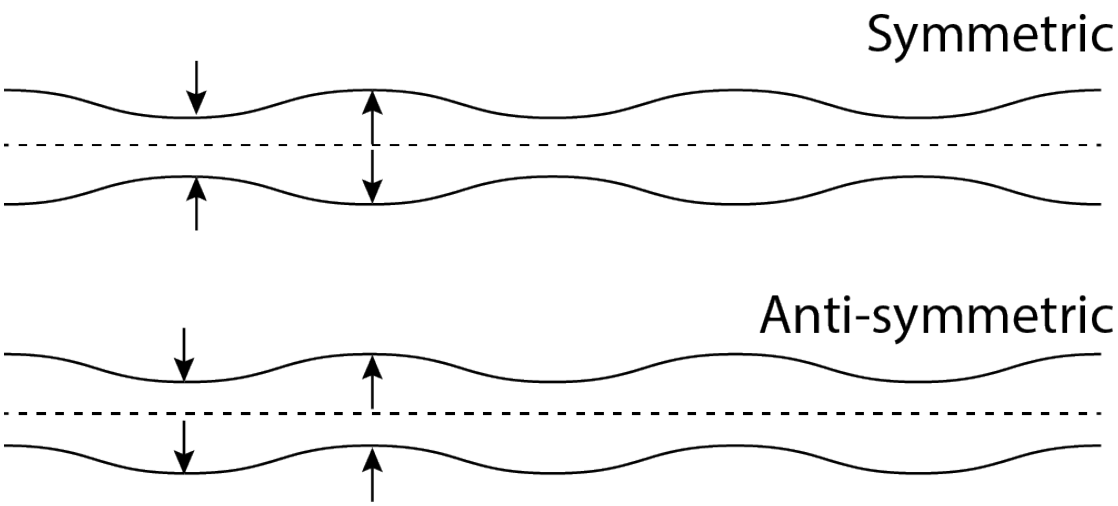

FIGURE 4.2: Example of a plate symmetric and anti-symmetric oscillation.

defect, it may give information on its severity and position. The presence and severity of damage and defects can be detected by assessment of the attenuation in the transmitted signal when compared to previous baseline measurements, and position information may be obtained by measuring the wave reflection as it encounters the acoustic interface produced by the defect or damage. Examples of damage detection include the works by Tang *et al.* [106], which employed the use of Lamb waves to detect fiber fracture, and by Seale at al. [107], using Lamb wave techniques to assess fatigue and thermal damage.

In literature, techniques for detection of damage through Lamb waves have been implemented in a variety of ways, including the use of separate sensors and actuators to monitor the transmitted and reflected waves, or multipurpose patches doing the emission and sensing of the reflected wave. Often, an array of sensors, measuring a combination of the transmitted and reflected signals can be used to pinpoint and evaluate the severity of damage in a material.

The earliest recognition of Lamb waves as a damage detection mechanism came in 1961 by Worlton *et al.* [96], reporting on the dispersion curves of aluminum and zirconium to analytically describe the characteristics of the various modes that could be useful for NDE applications, discussing also the motions and velocities of the interior particles, and the effects of holes and of varying thicknesses on the waveform. This led to the later development of the first potential aerospace application, as introduced by Demer and Fentnor [108], citing ultrasonic wave testing as one of the most reliable forms of NDE, and the emergent Lamb waves as an emergent way to acquire information about the medium's density, thickness and elastic properties. Their work consisted of locating fatigue cracks in stainless-steel and aluminum rods by recording the time-of-flight and attenuated amplitude of the received reflected and transmitted signals. Lamb waves then evolved to application in composite materials, as research at NASA by Saravanos

et al. demonstrated analytically and experimentally the ability of Lamb waves to detect delamination in composite beams [109, 110]. Similar results were replicated by Percival and Birt [100, 101], shifting the focus of the investigation on the first two fundamental Lamb wave modes. Each emitted propagation mode and frequency were later shown to present different sensitivities to different kinds of defects (*e.g.* A0 is more sensitive to surface defects; wavelength of selected mode must be lower than or equal to the size of damage [102] for detection to be possible).

Commonly, Piezoelectric lead zirconate titanate (PZT) crystals can be used for both generation and acquisition and are a cheap, easy to integrate solution for in-situ inspection. Some of the limitations of these sensors come from the nonlinear behavior under conditions such as large strains and temperatures and their low fatigue life and brittleness. Important work on the optimization of directional Lamb wave generation was conducted by Cawley *et al.* [111, 112] with the development of flexible and cheap Polyvinylidenedifloride (PVDF) transducers to generate and detect the waves. These emitters show the ability to generate highly focused and directional waves without producing higher mode interference, as was shown on various metallic specimens with encouraging results. Reciprocally, Soutis *et al.* focused on the optimization sensor placement and signal processing of the waves [113–115], while choosing PZT actuators over the PVDF counterparts due to the voltage requirement advantages.

Optical fiber sensors have also been considered due to the lightweight, immunity to EMI, long life and low power consumption and cost. Particularly, FBGs have been used for this purpose. One early limitation is the low sampling rate of wavelength measurements, which can be circumvented by means of using a photodetector and a tunable laser coupled with the FBG, effectively converting the sensing into an intensity measurement. Teixeira *et al.* [116] summarized the dominant technologies and recent developments in optical sensors for acoustic applications, and evaluated each of the techniques advantages and drawbacks. Once again, FBGs hold a strong advantage for embedding purposes due to the multiplexing ease and lack of intrusiveness as intrinsic sensors. The use of fiber Bragg gratings as damage detectors in composites using Lamb waves was demonstrated by Miesen *et al.* [117], using prepreg composite plates and bonded FBG. The group studied the velocity of the Lamb waves along the direction of the reinforcement and at 90º to it, and verified that the wave distorted and reduced velocity in the presence of cracks. The work concludes that FBG can be used for lay-up monitoring of prepreg plates. The observed sensitivity of FBGs to a mechanical wave is vastly dependent on orientation relative to the wave propagation as shown by Kessler *et al.* [118], and to its bonding: glued FBGs present a sensitivity up to 20-times lower than that of embedded ones [119].

The conducted work features the assessment of FBG sensors as alternatives to PZT crystals, comparing the wave response and sensitivity to a simulated surface defect.

Part III

Experimental Methods and Results

CHAPTER 5

Real-time monitoring of physical parameters in composite plates

The previous sections set the theoretical background and exposed the work that has been previously done regarding the studied subject. The following section of this work deals with the monitoring of the cure process and real-time in-situ monitoring of physical parameters. A novel embedded sensor head involving local alteration of the material properties by using different surrounding ply orientation for each pair of FBGs is designed and presented, using the same sensors for the monitoring of the plate manufacture. The mechanical response of the proposed design was thoroughly simulated prior to any test using *ABAQUS-CAE* finite element analysis (*Dassault Systèmes*), to predict the behavior of the plate to tensile and three-point bending tests. The sensor provides the possibility for simultaneous measurements of temperature/curvature and temperature/strain.

For this end, three samples were produced over the course of the work. The first two were used for the monitoring of manufacture and for assessment of the lay-up techniques. The remaining was produced using a different egress method for the sensors, and used for both the manufacture monitoring and for the mechanical and temperature characterization, and evaluation of the sensor head.

5.1 Sensor Design

A fiber Bragg grating's reflected spectrum consists of narrow band around the Bragg wavelength determined by equation 3.5, which is found to be a function of the effective modal index (n_{eff}) and the grating's period length (Λ). Variations on each of these parameters will induce a shift in the reflected spectrum, as occurs when strain or temperature change is applied to the fiber. From equation 3.6, the temperature induced shift, therefore, is obtained by:

$$\Delta\lambda_B^T = \lambda_B(\alpha + \xi)\Delta T \tag{5.1}$$

where α is the coefficient of thermal expansion of the fiber material, and ξ the fibre thermo-optic coefficient.

The longitudinal strain induced shift is given by:

$$\Delta\lambda_B^\varepsilon = \lambda_B(1 + \rho_\alpha)\Delta\varepsilon \tag{5.2}$$

$\rho_\alpha = \frac{n^2}{2} \cdot [\rho_{12} - \nu \cdot (\rho_{11} + \rho_{12})]$ being the photoelastic coefficient, where ρ_{12} and ρ_{11} are the components of the fiber-optic strain tensor and ν is the Poisson's ratio. For purposes of strain and temperature measurement, these equations can be further simplified to

$$\Delta\lambda_B^T = \kappa_T\Delta T \quad \text{and} \quad \Delta\lambda_B^\varepsilon = \kappa_\varepsilon\Delta\varepsilon \tag{5.3}$$

$$\Delta\lambda_B = \Delta\lambda_B^\varepsilon + \Delta\lambda_B^T \tag{5.4}$$

with κ_T and κ_ε being the temperature and strain sensitivities for each FBG sensor. In this work's specific case, to solve the cross-sensitivity problem a pair of FBGs are embedded in a composite plate which consists of a stack of five layers of unidirectional CFRP with two sections, each with a different stack orientation: (0-0-0-0-0) and (0-90-0-90-0). This changes the FBGs strain and temperature response due to the different surrounding material properties, enabling simultaneous measurement of temperature and strain. With two sensors, using equation 5.4 for each of them, one arrives to the following system of equations:

$$\begin{cases} \Delta\lambda_{B1} = \Delta\lambda_{B1}^\varepsilon + \Delta\lambda_{B1}^T \\ \Delta\lambda_{B2} = \Delta\lambda_{B2}^\varepsilon + \Delta\lambda_{B2}^T \end{cases} \tag{5.5}$$

Which, by plugging in equation 5.3 can be rewritten in matrix form as

$$\begin{bmatrix} \Delta\lambda_1 \\ \Delta\lambda_2 \end{bmatrix} = \begin{bmatrix} \kappa_{T1} & \kappa_{\varepsilon 1} \\ \kappa_{T2} & \kappa_{\varepsilon 2} \end{bmatrix} \begin{bmatrix} \Delta T \\ \Delta\varepsilon \end{bmatrix} \tag{5.6}$$

This, in turn, can be solved for temperature and strain shift,

$$\begin{bmatrix} \Delta T \\ \Delta \varepsilon \end{bmatrix} = \frac{1}{D} \begin{bmatrix} \kappa_{\varepsilon 2} & -\kappa_{\varepsilon 1} \\ -\kappa_{T2} & \kappa_{T1} \end{bmatrix} \begin{bmatrix} \Delta \lambda_1 \\ \Delta \lambda_2 \end{bmatrix} \tag{5.7}$$

The matrix $\begin{bmatrix} \kappa_{\varepsilon 2} & -\kappa_{\varepsilon 1} \\ -\kappa_{T2} & \kappa_{T1} \end{bmatrix}$ is known as the sensor matrix, with D being its determinant $D = \kappa_{\varepsilon 2}\kappa_{T1} - \kappa_{\varepsilon 1}\kappa_{T2}$. By knowing the sensitivities of each sensor and solving the system of equations, a discrimination can be made between the induced temperature and strain shifts. Obviously, this is only possible for $D \neq 0$. In general, provided that $\frac{\kappa_{T1}}{\kappa_{T2}}$ is sufficiently different from $\frac{\kappa_{\varepsilon 1}}{\kappa_{\varepsilon 2}}$, accurate discrimination can be obtained.

Similarly, the sensor can be shown to work for curvature. Curvature is defined as the reciprocal of the radius, which can be expressed as a function of the length of the sample and it's maximum deflection from a purely geometrical standpoint as:

$$R = \frac{(\frac{L}{2})^2 + h^2}{2h} \tag{5.8}$$

R being the radius, h the maximum deflection and L the gauge length. As h increases, the strain experienced in the sample around the deflection point will also increase. Since h varies proportionally to the strain at any fixed point in the sample, we can define h as:

$$h = \frac{\Delta \lambda_B^{\varepsilon}}{\kappa_h} \tag{5.9}$$

κ_h being a deflection coefficient that correlates the maximum deflection to the wavelength shift. Plugging this back in equation 5.8 gives:

$$R = \frac{(\frac{L}{2})^2 + (\frac{\Delta \lambda_B^{\varepsilon}}{\kappa_h})^2}{2\frac{\Delta \lambda_B^{\varepsilon}}{\kappa_h}} \tag{5.10}$$

which, as curvature, can be written as:

$$C = \frac{2\frac{\Delta \lambda_B^{\varepsilon}}{\kappa_h}}{(\frac{L}{2})^2 + \frac{\Delta \lambda_B^{\varepsilon}}{\kappa_h}^2} \tag{5.11}$$

For small deflections, that is $h^2 \ll (\frac{L}{2})^2$, the function can be approximated as linear.

$$C(\Delta \lambda_B^{\varepsilon}) \cong \frac{2}{\kappa_h \cdot (\frac{L}{2})^2} \Delta \lambda_B^{\varepsilon} = \frac{1}{\kappa_C} \Delta \lambda_B^{\varepsilon} \tag{5.12}$$

κ_C being the sensor coefficient to correlate the shift to temperature. Having two sensors with different curvature and temperature coefficients, a system of equations can be solved in the same way as previously (for strain and temperature) in order to attain simultaneous measurement of temperature and curvature.

$$\begin{cases} \Delta\lambda_{B1} = \Delta\lambda_{B1}^{C} + \Delta\lambda_{B1}^{T} \\ \Delta\lambda_{B2} = \Delta\lambda_{B2}^{C} + \Delta\lambda_{B2}^{T} \end{cases} \tag{5.13}$$

which in turn can be written in matrix form as

$$\begin{bmatrix} \Delta\lambda_1 \\ \Delta\lambda_2 \end{bmatrix} = \begin{bmatrix} \kappa_{T1} & \kappa_{C1} \\ \kappa_{T2} & \kappa_{C2} \end{bmatrix} \begin{bmatrix} \Delta T \\ \Delta C \end{bmatrix} \tag{5.14}$$

and solved for the temperature and curvature shift, arriving at:

$$\begin{bmatrix} \Delta T \\ \Delta C \end{bmatrix} = \frac{1}{D} \begin{bmatrix} \kappa_{C2} & -\kappa_{C1} \\ -\kappa_{T2} & \kappa_{T1} \end{bmatrix} \begin{bmatrix} \Delta\lambda_1 \\ \Delta\lambda_2 \end{bmatrix} \tag{5.15}$$

And thus finding the sensor matrix for simultaneous measurement of temperature and curvature, D being defined as $D = \kappa_{C2}\kappa_{T1} - \kappa_{C1}\kappa_{T2}$.

In both cases, the greater the matrix determinant, the better the accuracy of the measurements [120].

5.1.1 Composite plate design and manufacture

Three rectangular plates of 300 mm x 50 mm x 2.5 mm (200 mm gauge length, 50 mm on each end for gripping), half unidirectional (0-0-0-0-0), and half bidirectional (0-90-0-90-0), with two FBGs embedded along its middle axis, were manufactured by vacuum assisted resin infusion moulding. The sample schematic can be seen in Figure 5.1.

The FBGs are embedded during the lay-up by weaving the fiber through the fabric to hold them in place during the required handling for the manufacture. These should be placed far from non-linear strain effect regions in the sample, which can be predicted by finite element simulations.

The whole vacuum assisted resin infusion process starts with mold cleaning, with acetone and mold cleaner, and application of three fine coats of release agent (approximately 1% resin). The mold is then transported to a lay-up room with controlled environment, beginning the lay-up process. The cut fabrics are stacked in the required

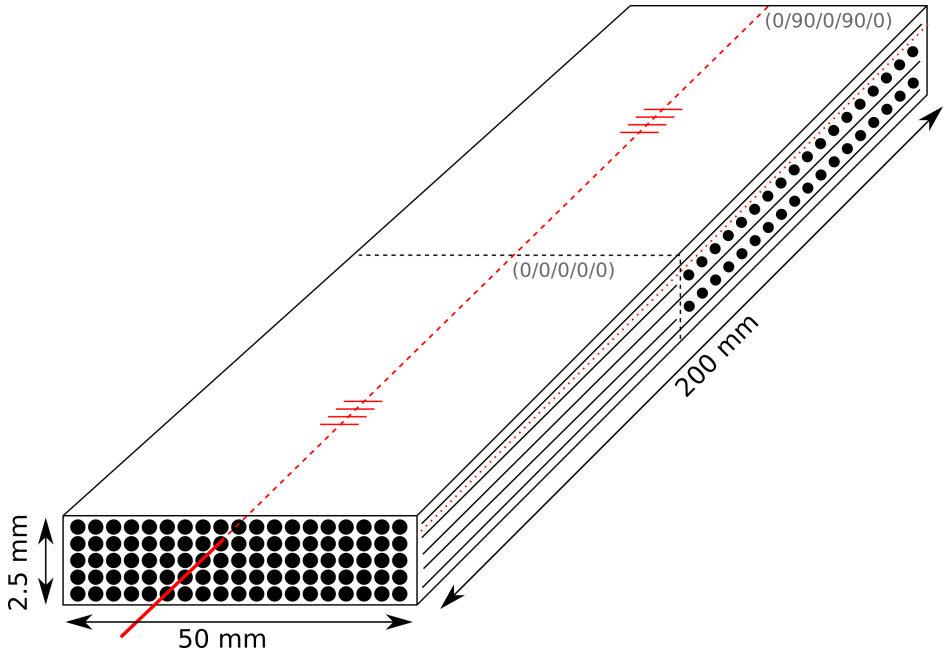

FIGURE 5.1: Schematic depiction of the produced hybrid uni/bidirectional sample.

order. A vacuum outlet and resin inlet are placed using spiral tube on opposing sides of the stacked fabrics. Peel-ply (fabric of porous nylon and silicone, to prevent adhesion of the mesh to the carbon fibers) is subsequently placed on top of the fabric, followed by a mesh which is used to facilitate the flow of resin across the fabrics.

Tacky-tape is then used to cover the edges of the mold and polymer tube is connected to the inlets and outlets. The mold is afterwards covered with a bagging film and pressed against the tacky-tape to prevent leaks, the inlet is blocked and vacuum is applied. This concludes the lay-up process. As the next step, the infusion process begins by carefully mixing the necessary amount resin and hardener in the right ratio. The mixture is later placed in a vacuum chamber, removing any air and bubbles, which is then connected to the resin inlet, and vacuum is applied to the bag, carrying the resin through the mesh and soaking the fibers. Once the infusion is complete, the inlets and outlets are sealed to keep the vacuum in the bag and the preform is then taken to a curing oven/plate or autoclave.

The sample was manufactured infusing five layers of *SigmaTex* unidirectional carbon fiber (T300C, 12K, 450 g/m^2) with *Araldite® LY 564* resin (low-viscosity epoxy resin) and *Aradur® 2954* hardener (cycloaliphatic polyamine) using the recommended 100:35 weight ratio. The employed fiber Bragg gratings were *SmartFibres SmartFBG* imprinted in Single Mode SMF-28, 9/125 μm fiber, with polyimide recoat at the sensor region. The layers were cut to the desired shape, with one of the (0) layers and the (90) oriented layer being cut in half for later stacking in the aforementioned fashion. For the manufacturing and prior to sensor embedding, all layers were stacked apart from the top layer.

The sensors were then woven through the fabric to ensure their position at the interface of the first and second lamina of the sample and prevent buckling during handling, and at 50-55mm from the center of the sample. These were egressed from the side with short PTFE (Polytetrafluoroethylene) tubes to protect the egress/ingress region. The final layer was carefully placed on top and the sample was vacuum bagged. The sensors were also egressed from the bag for monitoring the manufacturing process. For the infusion, the amount of resin was calculated in order to have 50% volume fraction.

The cure was subsequently performed in a curing oven, using the cure cycle depicted in Figure 5.2.

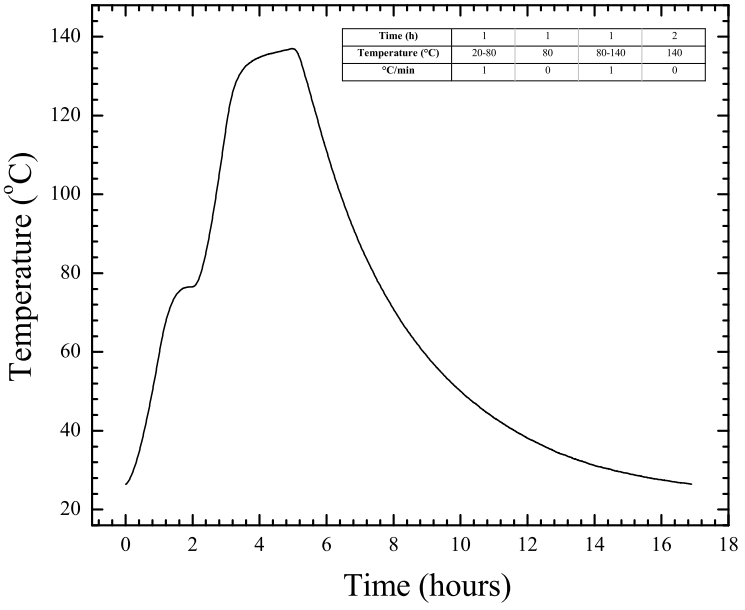

FIGURE 5.2: Cure cycle used for the sample manufacture.

5.1.1.1 Egressing the sensors

The first two samples were done simultaneously (on the same plate, to be later cut to size) egressing the sensors from the top of the sample (out-of-plane), in order to allow posterior tailoring of the plate shape (to divide the two samples, and to eliminate tapering at the edges) by means of cutting and sawing. After the manufacture, during the debagging, specifically during the removal of the peel-ply, two of the sensors broke at the embedding sections as a result of the mesh and peel-ply adhering to the sensor entry, and the cured resin rending the sensors and protective tube brittle. This egress method was consequently deemed unreliable, so the following sample was done by egressing the sensors from the edge of the plate, which proved successful. Since there is

no contact of the ingress section with the mesh, the sensor ingress region isn't subjected to as much force during the removal of the peel-ply, nor does it have as much cured resin (the amount it has is easily removable by scraping). In all cases the region of ingress was protected by a short PTFE tube. Figure 5.3 shows the third sample, being possible to see the ingress/egress region.

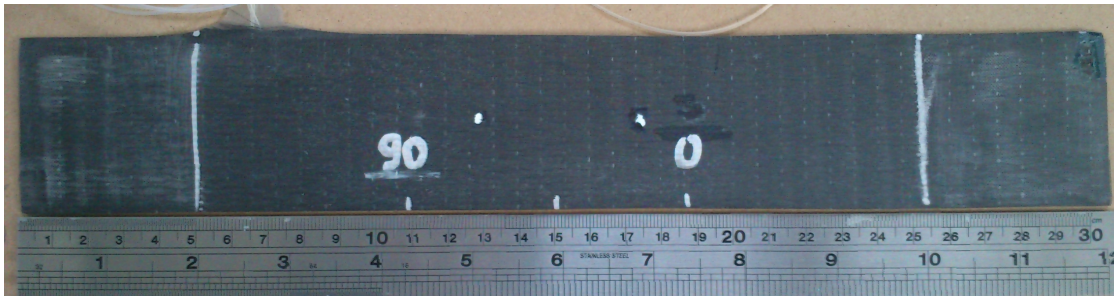

FIGURE 5.3: Third sample photo. Note the egress/ingress region (top-left) from the side of the laminate. 90 represents the bidirectional and 0 the unidirectional section, white lines mark the gauge length and the white dots are used as reference points for the AVE strain measurements.

5.1.2 Simulations

The engineering constants of the sample used for the simulations were calculated by using the rule of mixtures (See Chapter 2), estimating 50% fiber/matrix volume fraction, amount for which the resin volume was calculated prior to the infusion process. The properties for fiber and matrix were obtained from the respective datasheets of *T300C* carbon fibers and *Araldite® LY 564/Aradur® 2954* mixture.

The engineering constants calculated (see table 2.1) for the simulation are those presented in table 5.1.

TABLE 5.1: Elastic constants for the FE simulation.

E_{11}	$E_{22/33}$	ν_{12}	ν_{23}	$G_{12/13}$	G_{23}
MPa	MPa	-	-	MPa	MPa
133 000	10 000	0.2	0.3	7000	8000

Regarding the tensile strain simulation, Figure 2 shows the finite element model (FEM) for the longitudinal strain (ε_{11}) and the position of the sensors. The simulation was done using 1.5x1.5x0.5, linear hexahedron type C3D8R elements, applying a tension load ramp to 10kN.

From the results, one concludes that, since FBGs have a linear response to strain, to ensure a linear response the sensors should be placed as far from the interface of the

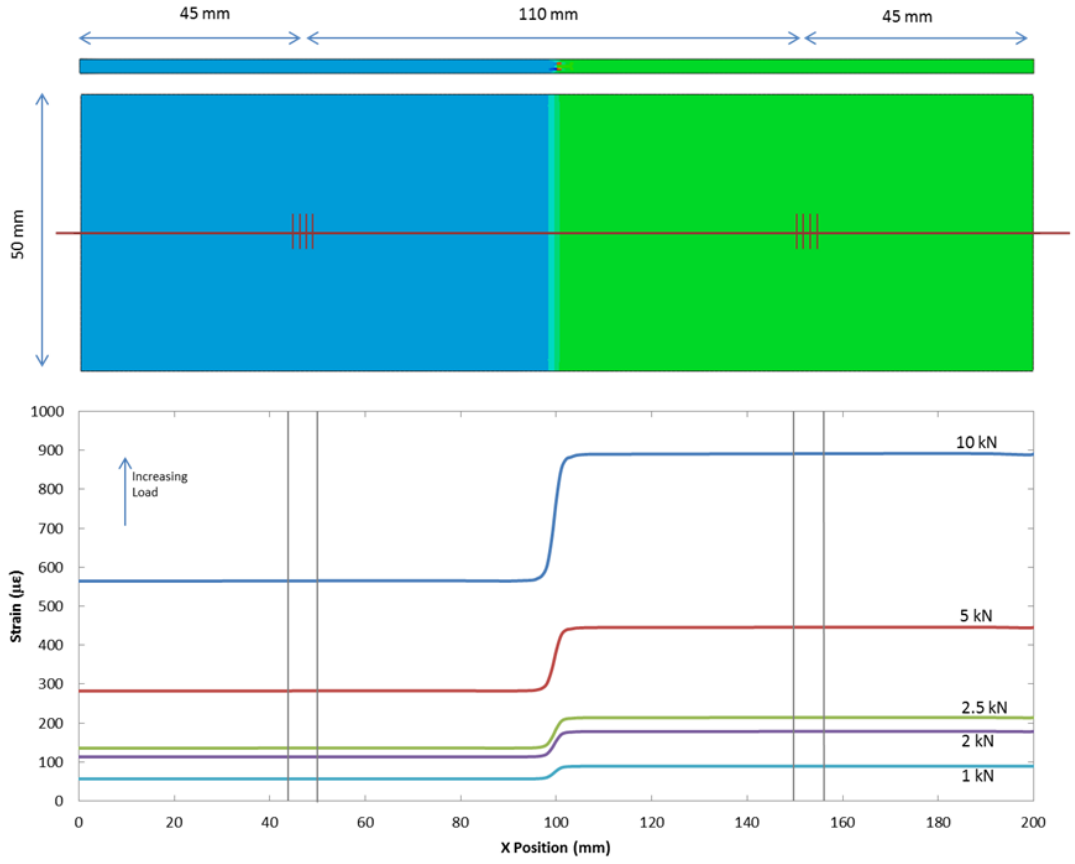

FIGURE 5.4: Longitudinal strain (ε_{11}) simulation as a function of the position on the sample, for a quasi-static tension test. The FBG location is clearly indicated.

two sections and from the edge of the gauge length as possible to prevent non-linear behavior due to gripping induced edge effects, which were not taken into accounted when performing the simulation. Additionally, the response close to the middle interface may also be more complicated than that depicted, as some slight fabric overlapping/gap may occur between the 90º and 0º fabrics.

This sample shows a significant increase in sensitivity on the (0-90-0-90-0) section, due to less longitudinal reinforcement, and a very abrupt strain gradient in the middle interface between the two sections. The sensors were placed approximately symmetrically at 50-55 mm from the center of the sample.

From the simulation one concludes that one major drawback of this design is the center interface which creates a stress concentration and weak point, due to different transverse strains between the bidirectional and unidirectional reinforced sections. Due to the non-linear strain response, this may also present an interesting zone for further study, but outside of the scope of this work.

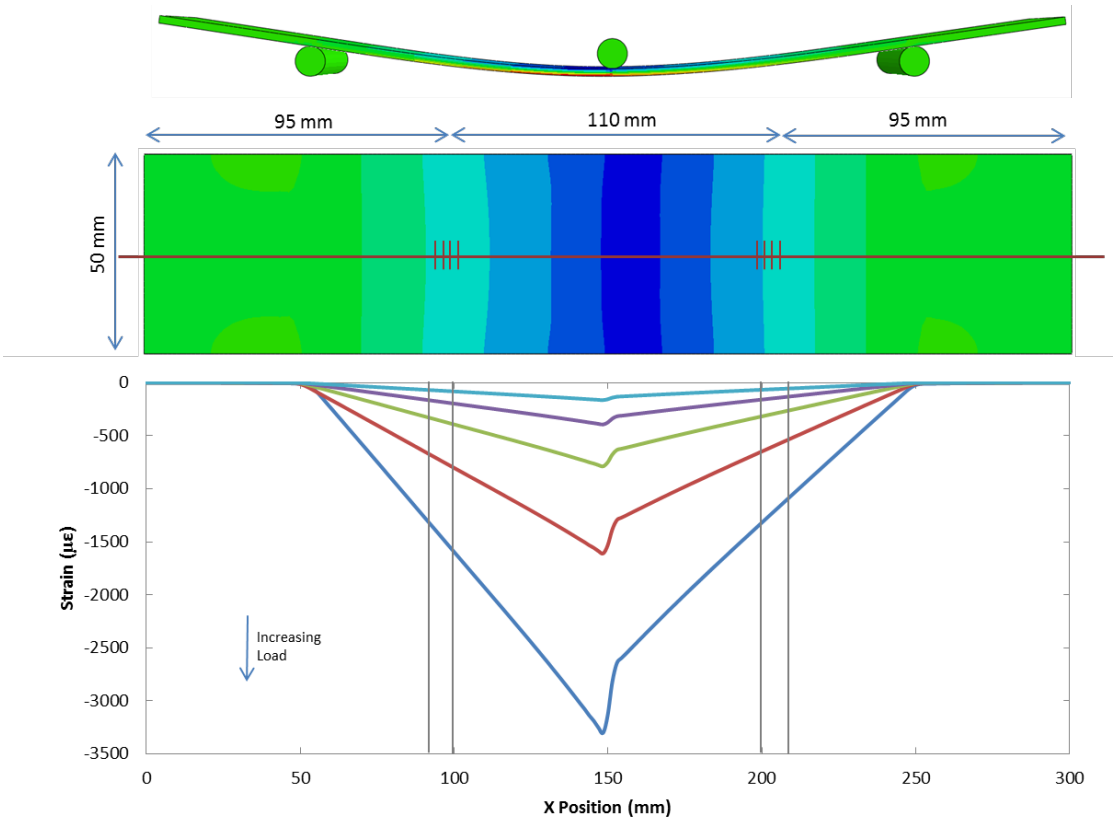

FIGURE 5.5: Curvature response simulation (three-point bending test) with longitudinal strain (ε_{11}) as a function of position. The represented results are for the loaded face (measuring compression).

For the curvature simulation, Figure 5.5 shows how the strain sensitivity of each FBG relates to its position on the sample as it is subjected to a bending load. Remarkably, unlike the tensile strain case, the position of each of the FBGs on the sample is very important to allow simultaneous measurement and eliminate the cross-sensitivity problem, which requires different sensitivities for each FBG, and as such they should be carefully placed in two places with distinct strain sensitivities. It's also worth noting that in the three-point bending test in particular, a strain gradient is observed along the plate sections, which may affect or distort the spectral response on the FBG. Ideally, the smaller the FBG, the least influence from the gradient will be felt. Additionally, since the sensors are placed close to one of the faces of the plate (between the two top layers), depending on which side is loaded a compressive or equivalent tensile load (*i.e.* symmetrical wavelength shifts) will be measured.

As mentioned for the plate fabrication, the sensors were placed approximately symmetrically at 50-55 mm from the center of the sample. The three bearings were simulated as isotropic (steel), with 5 mm radius. Once again, the simulation was done using

1.5x1.5x0.5, linear hexahedron type C3D8R elements. The surfaces of the sample interact with the three 5mm radius bearings, the middle one applying the load. Both sections show different strain responses, with the measured compressive strain increasing as it approaches the middle of the sample, where the load is applied.

5.2 Manufacture Monitoring

FBGs are sensitive to strain and temperature: In order to discriminate both parameters and obtain accurate strain results for the monitoring of the plate's curing cycle, a thermocouple (see Appendix A) was used. Knowing the temperature sensitivity of the sensors (previously characterized), the temperature reference may be used to isolate the strain measurements. Multiplication of the thermocouple-obtained temperature variation by the calibrated thermal sensitivity κ_T of the optical fiber yields the strain response.

$$\Delta\varepsilon = \frac{1}{\kappa_\varepsilon}(\Delta\lambda_1 - \kappa_T \Delta T_{Thermocouple}) \tag{5.16}$$

The thermocouple's intrusiveness makes the concept unsuitable for out-of-lab applications, but it's a convenient and practical method for cure monitoring applications. For this purpose, datasheet values of the FBG temperature sensitivity were used (11 pm $\cdot^o C^{-1}$).

The sensors were egressed from the bag, with the fiber protected from the resin using PTFE tube. The connectors were then accessed via a small door in the curing oven for the purpose of monitoring. The thermocouple was fixed with tape to the middle of the sample surface.

All FBG measurements were done using a *SmartFibres W4 FBG* Interrogator (*MicronOptics sm125-500* model) with 1Hz maximum scan frequency and 1 pm wavelength accuracy, using *MicronOptics Enlight* software. Reference temperature measurements were done using K-Type (chromel-alumel) *Picolog* Thermocouples, and a *Picolog TC-08 Thermocouple Data Logger*, connected to PLW Recorder Software, with $\pm 0.5^{o}C$ temperature accuracy.

5.2.1 Results

The first two samples were manufactured simultaneously (in the same plate). The results are shown in figures 5.6.

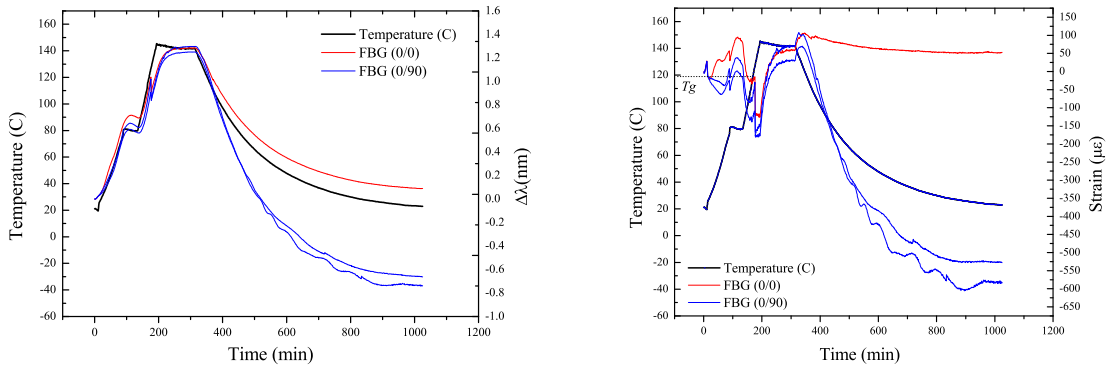

(A) FBGs measuring strain and temperature. (B) FBGs with temperature effect removed.

FIGURE 5.6: Simultaneous monitoring of the first two samples.

The sensor at the (0/0) interface for one of the samples was damaged during the manufacture and as a result there is no information regarding sample 1 unidirectional section. All interrogated sensors at the start closely follow the thermocouple's behavior, up until $120C$, when an abrupt change is verified. After removing the temperature measurement from the sensor response, we see the abrupt compressive strain around $120C$, followed by a tension back to neutral strain. This corresponds with the T_g (Temperature at which the glass transition is expected to occur for the specified cycle - $123 - 127C$ according to the used epoxy's datasheet) and as such, the measurements should correspond to the phase change inside the sample, leading to such a random strain behavior. Following the stabilization the sensor's embedded at the bidirectional interface appear to compress as the sample cools, creating a compressive residual strain of around 550 microstrain . The sensor at the unidirectional interface appeared to not suffer any noteworthy compressive or tensile strain (50 microstrain) during the cure, and does not show any residual strain posterior to the manufacture.

These results are in accordance with previous studies [8], which verified a final compressive strain transverse to the reinforcement, while barely any compressive strain measured longitudinal to the reinforcement. Following these results, it's expected that sensors at the bidirectional interface will suffer a higher compressive strain. Additionally, from the obtained results it's apparent that the residual strains were derived from the sample compression during the cooling.

The third sample showed the results presented in figures 5.7

Once again the appearance of an abrupt strain change at a similar temperature from before is apparent, with an compression at around $100C$, corresponding to the T_g. The random strain behavior around this temperature is attributed to the phase change occurring to the epoxy, as in the previous sample's case. It is unclear why the glass transition

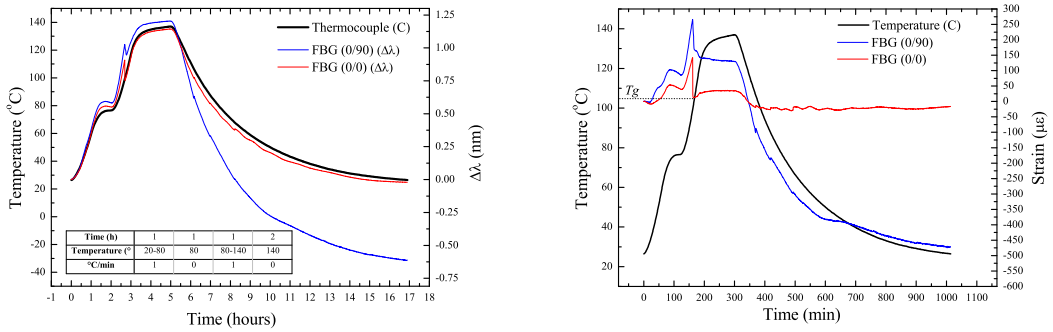

(A) FBGs measuring strain and temperature. (B) FBGs with temperature effect removed.

FIGURE 5.7: Monitoring of the third sample.

for this sample occured at a different temperature from the other two, but it can be related to the age of the epoxy, or due to it having spent more time in cup already mixed with the hardener. Once the sensor's strain behavior stabilizes, it's noteworthy that once again the sensor at the unidirectional interface barely suffers any sort of strain during the curing, while a compressive strain of around 500 microstrain forms in the bidirectional interface as the sample cools.

TABLE 5.2: Summary of observed T_g and residual strains during the cure monitoring.

	Tg	**Residual Strain**	
		(0/0)	(0/90)
Sample 1	120 C	no data	$-527\mu\varepsilon$
Sample 2	120 C	$52\mu\varepsilon$	$-583\mu\varepsilon$
Sample 3	100 C	$-16\mu\varepsilon$	$-470\mu\varepsilon$

Table 5.2 presents a summary of all the parameters obtained from the monitoring. The glass transition was observed in all samples and while the sensors at the unidirectional interface presented nearly no residual strains post-cure, at the bidirectional interface there is a gradual increase in residual strain as the resin cools down, likely due to the polymerization of the matrix.

5.3 In-situ real-time simultaneous measurement of physical parameters

After the monitoring of the cure process, the sample was debagged and the sensor response was characterized in order to find the strain, temperature and curvature coefficients. For the effect, all FBG measurements were done using a *SmartFibres W4 FBG Interrogator* (*MicronOptics sm125-500* model) with 1Hz maximum scan frequency and 1 pm wavelength accuracy, using *MicronOptics Enlight* Software for the acquisition. Reference temperature measurements were done using K-Type (chromel-alumel) *Picolog* Thermocouples, and a *Picolog TC-08* Thermocouple Data Logger, connected to *PLW Recorder Software*, with $\pm 0.5^{o}C$ temperature accuracy.

5.3.1 Temperature Response

The temperature characterization was performed by doing a temperature sweep from 20 C to 80 C in an *ELKOM vacuum press* (No vacuum applied), without any tensile or compressive loads applied to the plate, letting the vacuum plate to slowly cool overnight. The vacuum press was chosen since it cools down slower, minimizing any hysteresis verified when plotting the temperature response of the FBG versus the temperature measured by the thermocouples (which are not embedded), due to the thermal lag created by the surrounding epoxy's thermal capacity. The thermocouples were taped to the surface of the sample, closest to the sensors.

Since the vacuum press heats the sample on one side only, to minimize the temperature gradient over the course of the sample, and keep the temperature as homogeneous as possible throughout the thickness, the sample was covered with some breather fabric.

Figure 5.8 shows the temperature response of the sensors during the whole cycle on the plate. As such, the thermal sensitivity analysis is done by plotting the FBG response against the temperature measured by the thermocouple. The results are presented in Figure 5.9, which shows the response and linear fit, and how the FBG sensors response changed after embedding in the composite plate.

Remarkably, the FBG sensors at the (0-90) interface showed an increase in sensitivity to temperature, which may be attributed to stress formed in the manufacturing of the plates at the interface between the 0 and 90 lamina, and local variations in the amount of resin surrounding the sensors [12]. The variation in sensitivity is found through the following equation

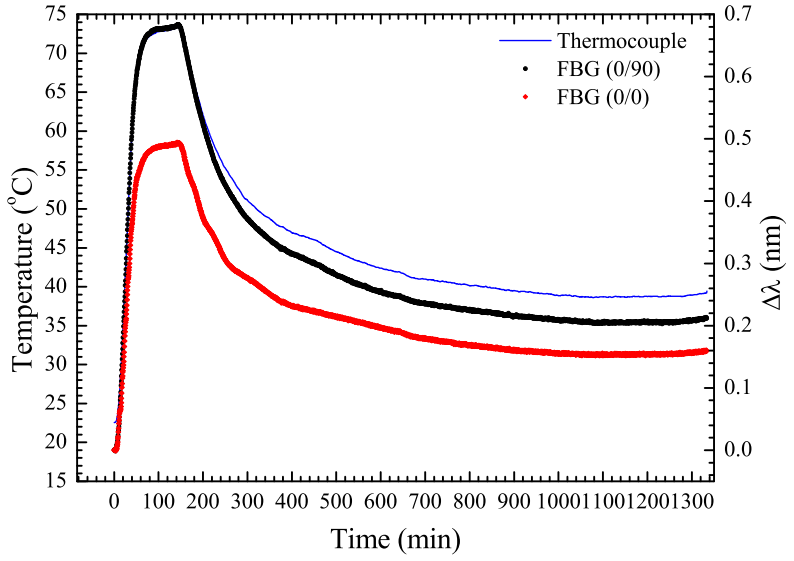

FIGURE 5.8: Time division multiplexing interrogation system example.

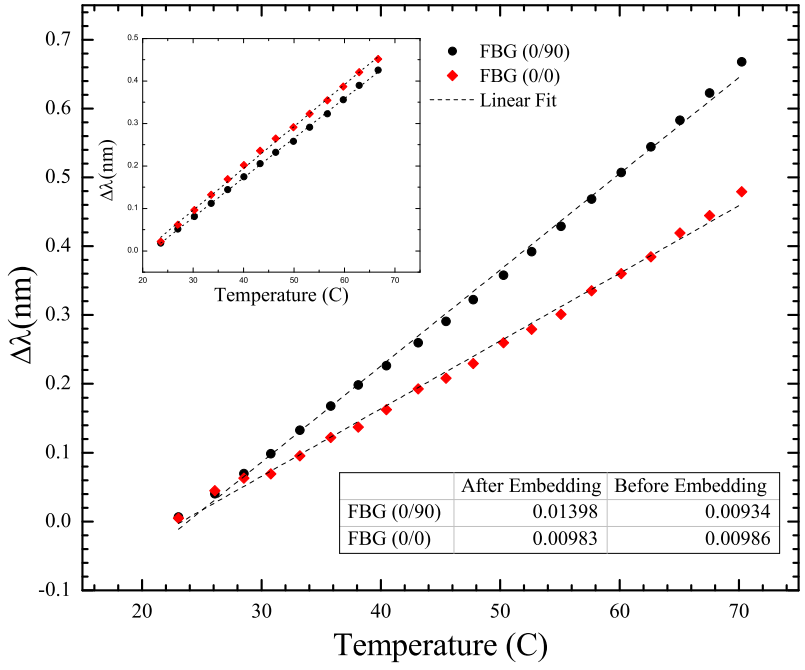

FIGURE 5.9: Temperature response for both FBG before (inset) and after embedding.

$$\frac{\kappa_T^{afterembedding} - \kappa_T^{beforeembedding}}{\kappa_T^{beforeembedding}} \tag{5.17}$$

At the (0-0) interface, the sensor showed the least change in its response (0.3%), while the sensor at the (0-90) showed a great increase in sensitivity (49.6%). From

this experiment, the thermal sensitivities of the embedded sensors are obtained as $\kappa_T^{0/0} = 9.83$ pm $\cdot^o C^{-1}$ for the sensor at the (0/0) interface, with a standard error measured as $\sigma_T^{0/0} = 0.147$ pm $\cdot^o C^{-1}$, and $\kappa_T^{0/0} = 13.98$ pm $\cdot^o C^{-1}$ for the one at (0/90), with standard error measured at $\sigma_T^{0/0} = 0.154$ pm $\cdot^o C^{-1}$.

5.3.2 Strain Response

Strain characterization measurement tests were done using a loading test machine (*Instron model 5982*), while keeping the plate at constant room temperature (23 C). Two cycles were done from 0 to 600 microstrain, and total strain of the sample was measured using an *Instron AVE* (Advanced Video Extensometer) axial strain system. The sample was loaded at 0.20 mm/min. The sample was not subjected to some initial cycles to overcome potential accommodation effect of FBG sensors to the host material, which may induce some deviations in measurement [121].

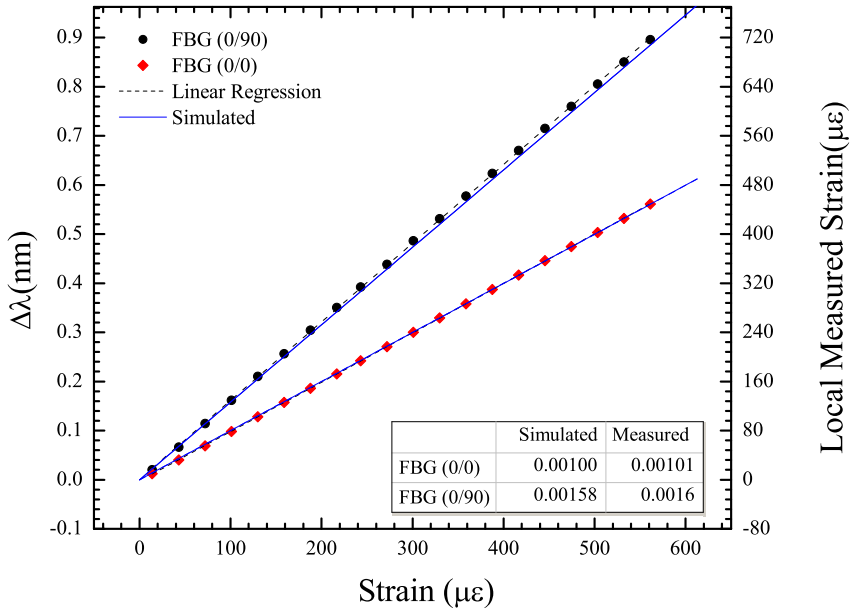

FIGURE 5.10: Experimentally obtained strain results for the quasi-static tension test, and the simulated results for comparison.

Figure 5.10 shows the results for the simulated and measured strain behavior of the sample. The AVE system used for reference strain experienced a measurement artifact at around 600 microstrain so the results are limited up to that range, although the loading was done up to 1000 microstrain. The simulated values were scaled to the (0-0) measurement, which showed the strain sensitivity of the sensors to be $\kappa_\varepsilon = 1.3$ pm $\cdot\, \mu\varepsilon^{-1}$.

The simulated strain ratios for the (0-0) and (0-90) section is 1.580 for the simulated values, and 1.584 for the measured values, being in excellent agreement. The sensitivities measured for each of the sensors at the (0/0) and (0/90) interface are $\kappa_\varepsilon^{(0/0)} = 1.0\ \text{pm} \cdot \mu\varepsilon^{-1}$ and $\kappa_\varepsilon^{(0/90)} = 1.6\ \text{pm} \cdot \mu\varepsilon^{-1}$, respectively, with standard errors $\sigma_\varepsilon^{(0/0)} = 6.25 \times 10^{-4}\ \text{pm} \cdot \mu\varepsilon^{-1}$ and $\sigma_\varepsilon^{(0/0)} = 3.36 \times 10^{-3}\ \text{pm} \cdot \mu\varepsilon^{-1}$.

5.3.3 Curvature Response

For curvature, the composite plate was measured using a three-point bending setup. The sample was loaded at a 1mm/min on an *Instron 5969* fitted with a 10kN load cell at constant room temperature (23 C). 5mm radius bearings were placed at the edges of the gauge length and the sample was loaded along its middle axis.

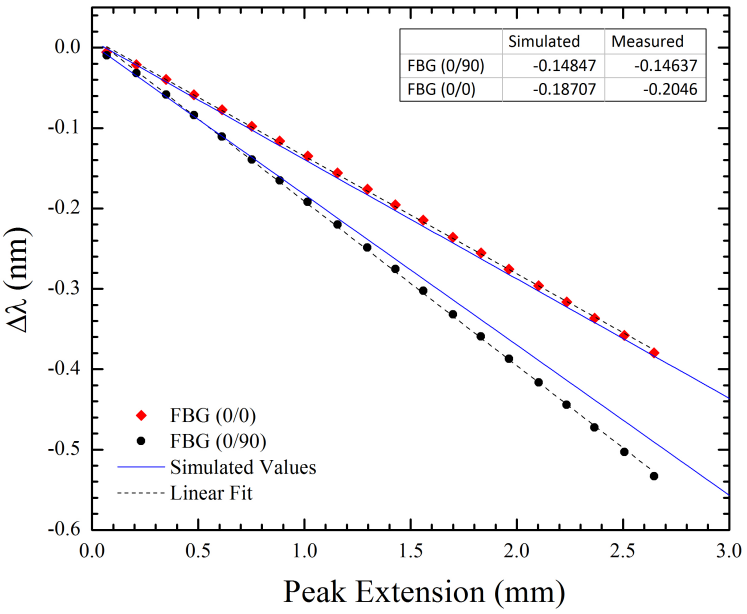

FIGURE 5.11: Wavelength shift as a function of the peak deflection (at the loading point of the sample) during a three point bending test.

The sample was loaded from 0mm to 3mm extension for the curvature measurements, then held and raised up to 5mm extension to measure the effects of the strain gradient on the FBG peak, which were found to be negligible for these extension lengths. The wavelength shift as a function of the peak extension can be found in Figure 5.11.

Plotting the wavelength shift as a function of curvature (Figure 5.12), according to equation 5.11 yields linear behavior for small curvatures ($h^2 << (L/2)^2$), and the coefficients

can be obtained as $\kappa_C^{(0/0)} = -732$ pm · m and $\kappa_C^{(0/90)} = -1024$ pm · m, with the standard errors $\sigma_C^{(0/0)} = 4.74$ pm · m and $\sigma_C^{(0/90)} = 3.56$ pm · m.

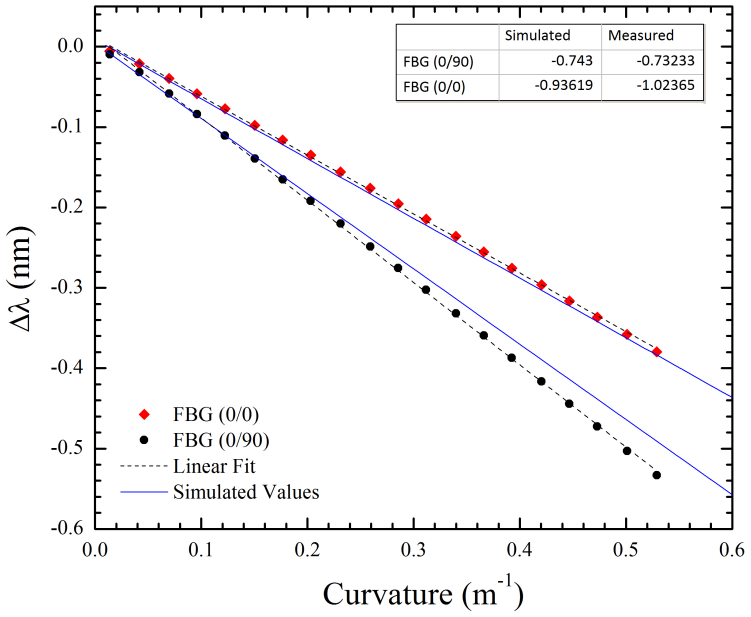

FIGURE 5.12: Curvature response of the sensors to a bending load, and simulated results for comparison, during a three-point bending test.

As expected, both sensors measure compressive strain since they are both placed on the loaded (concave) side of the loaded sample. The ratio of simulated strain for both sections is 1.260, while the ratio of sensitivities for the measured values is 1.398. The discrepancy in the simulation and experimental values may be attributed to displacements of the FBGs during the manufacturing in relation to the expected position, which may leave them asymmetrically placed on the sample.

5.3.4 Simultaneous Measurement

The proposed design exhibits different sensitivities to both temperature and strain/curvature, using similar FBGs. As such, it's possible to obtain a sensor for simultaneous measurements of strain and temperature or curvature and temperature using this type of composite plate.

Table 5.3 summarizes the coefficients and standard errors for the sample.

From equations 5.7 and 5.15, one derives the following solution for simultaneous measurement of strain and temperature:

TABLE 5.3: Sensor temperature, strain and curvature sensitivities.

	Temperature ($\text{pm} \cdot^o C^{-1}$)		Strain ($\text{pm} \cdot \mu\varepsilon^{-1}$)		Curvature ($\text{pm} \cdot \text{m}$)	
	κ_T	σ_T	κ_ε	σ_ε	κ_C	σ_C
(0/0)	9.83	0.147	1.0	6.25×10^{-4}	-1024	4.74
(0/90)	13.98	0.154	1.6	3.36×10^{-3}	-732	3.56

$$\begin{bmatrix} \Delta T \\ \Delta\varepsilon \end{bmatrix} = \frac{1}{1.748} \begin{bmatrix} 1.6 & -1.0 \\ -13.98 & 9.83 \end{bmatrix} \begin{bmatrix} \Delta\lambda_1 \\ \Delta\lambda_2 \end{bmatrix} \tag{5.18}$$

and the following for simultaneous measurement of curvature and temperature:

$$\begin{bmatrix} \Delta T \\ \Delta\varepsilon \end{bmatrix} = \frac{1}{167.44} \begin{bmatrix} -1024 & 732 \\ -13.98 & 9.83 \end{bmatrix} \begin{bmatrix} \Delta\lambda_1 \\ \Delta\lambda_2 \end{bmatrix} \tag{5.19}$$

For these coefficients, the wavelength is measured in pm, retrieving the temperature in Celsius, the strain in $\mu\varepsilon$ and the curvature in m^{-1}.

CHAPTER 6

Acoustic methods for defect and damage detection

The following section regards the use of FBG sensors in high-frequency applications for use in the evaluation of damages and defects in composites, namely the use of ultrasonic waves propagated through the material. This introduces a new set of challenges in comparison to the previous study of quasi-static tensile/bending strains and temperature was studied, for the monitoring of composites during operation and manufacture. The acquisition method and required signal processing are detailed, and the obtained results from the FBG are compared and validated with results from piezoelectric sensors, which have been more extensively studied in the literature for the purpose of Lamb wave detection.

The following study involves a characterization and comparison of FBG transverse and longitudinal response, assessment of sensitivity to different vibration modes of the material, and detection of a simulated defect's presence by the attenuation caused in the transmitted wave, as a function of the wave frequency and defect relative position (to the emitter). The group velocity measured for the wave propagation, and is compared to numerically simulated dispersion curves for the used material, as a way to better identify the propagation modes.

6.1 Plate properties and sensor bonding

The experiments were done in a 820 mm x 820 mm x 2.5 mm composite quasi-isotropic CFRP plate, with the following stack orientation (0/45/90/-45/0).

All the piezoelectrics were *PI Ceramic* PZT disks of 10 mm outer diameter and 0.5 mm thickness, and the employed fibre Bragg gratings were *SmartFibres SmartFBG* imprinted

in polyimide coated Single Mode SMF-28, 9/125 μm fibre, with polyimide recoat at the sensor region.

The piezoelectric emitters were bonded in the middle of the top and left side of the plate, at 150 mm distance from the edge. One third piezoelectric and FBG were bonded to the middle of the sample (at 260 mm from the two emitter piezoelectrics). The sensors were bonded with low viscosity glue after thoroughly sanding and cleaning the surface to promote good adhesion.

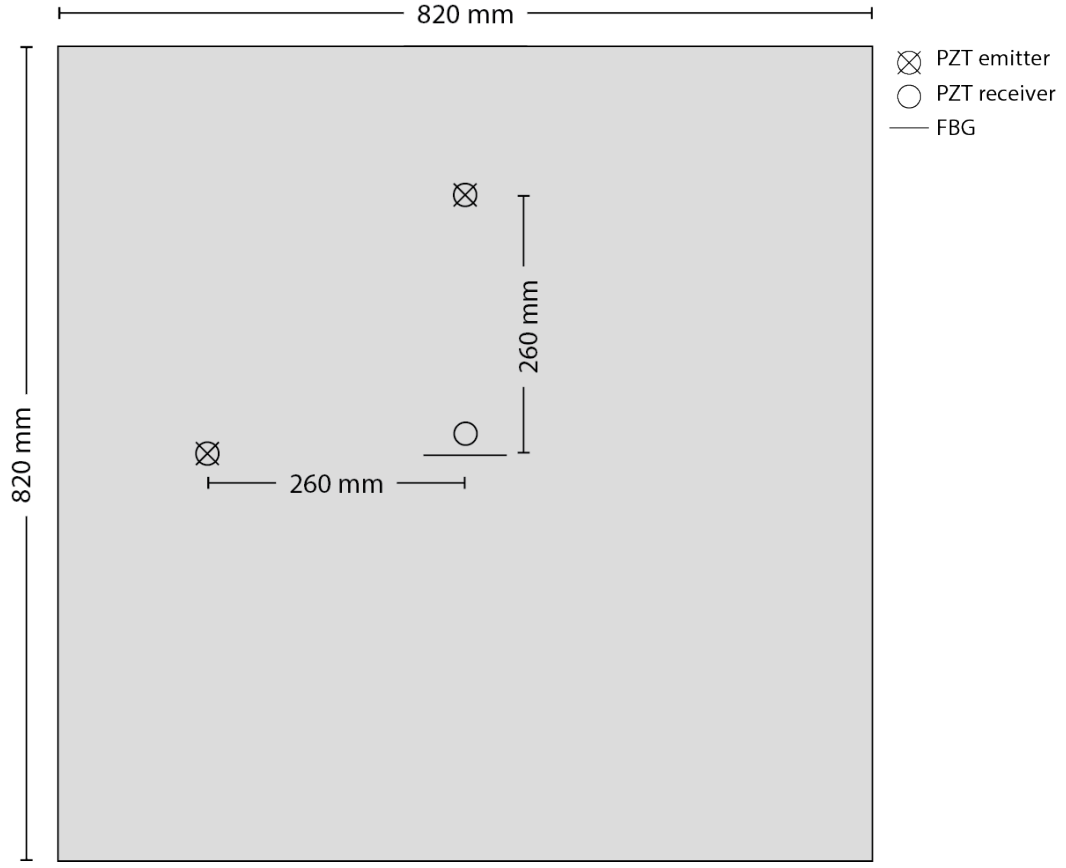

FIGURE 6.1: Drawing of the plate used for the test.

The emitter and receivers were connected to a *Tektronix 5034B* oscilloscope, triggered by the emitter signal in order to perform the measurements.

6.1.1 Damage detection setup

For the detection of a defect, the previous plate and sensors were used. The defect was simulated by using a 5 pence (pound sterling) coin, weighing 3.415mg and measuring 9mm in radius. The coin was covered in *Henley's* acoustic gel to improve coupling of the acoustic wave from the material to the coin.

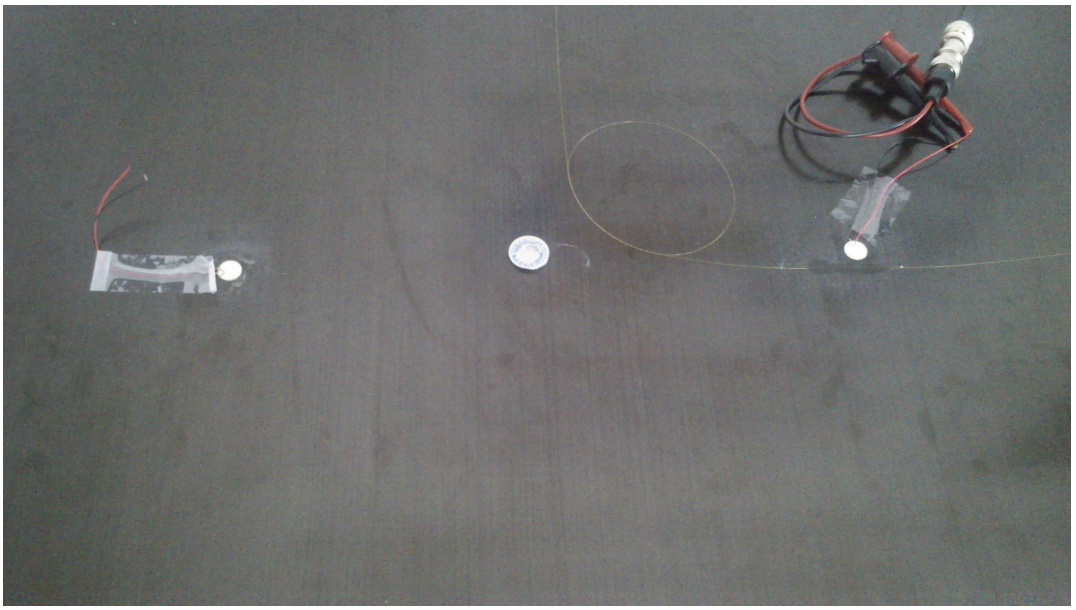

FIGURE 6.2: Plate with the bonded sensors and simulated defect in place.

The defect was placed at 130mm from the emitter (half way from the emitter to the receiver) longitudinal to the FBG orientation.

6.2 FBG interrogation and signal processing

Unlike the previous measurements performed with the FBG, which were performed by sending a wide light spectrum into the fiber, and observing the reflected peak's maximum deviation at 1Hz aquisiton rate, for the effect of measuring ultrasonic waves higher data speed acquisition is required, since the sent wavepackets will be on the 10kHz-500kHz frequency range. The chosen method to tackle the problem was to take advantage of the fact that the maximum induced shift from the vibration is lower than the width of the peak, and as such it's possible to employ a photodetector and convert the wavelength shift into an intensity measurement.

To do this, a tunable laser with a narrow band (*Thorlabs T200C*) was used. The laser was connected to a *Thorlabs 6015-3-APC* Fiber Optic Circulator, which connected to the FBG (through a *Thorlabs ADAFC3 FC/APC-FC/APC* mating sleeve) and finally to a *Thorlabs PDA10CS-EC* InGaAs photodetector. Figure 6.3 illustrates the setup.

Having this set up, by tuning the laser emission to one of the sides of the FBG peak any wavelength shift in the reflected FBG spectrum will cause a variation of the light intensity on the photodetector, which can promptly be observed on the oscilloscope.

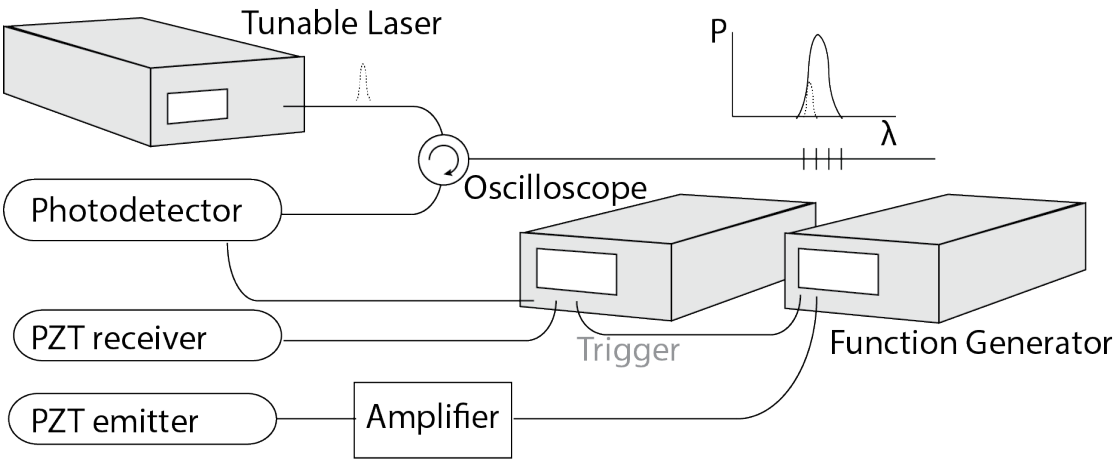

FIGURE 6.3: Interrogation system for the sensors bonded on the plate.

In order to improve the acquired FBG and PZT signal's signal-to-noise ratio (SNR), each measurement (triggered by the function generator emitted wave) was averaged 500 times on the oscilloscope. This also removes some random low-frequency fluctuation effects measured by the FBG due to local temperature variations.

The acquired signals are post-processed in *MatLab*. The acquired signal from the FBG has a bias value due to the average intensity of light incident on the photodetector, which must first be removed. The FBG measurements are run through a Hanning window band-pass filter to further remove low-frequency noise due to temperature oscillations and the laser-peak not being locked-in to the FBG spectrum. The peaks corresponding to the A0 and S0 emission are then found by running local maximum search algorithm on the Hilbert transform of the processed signals, removing peaks formed from reflections by introducing a threshold as a percentage of the absolute maximum. An example of the emitted and received signals is presented in Figure 6.4.

The output and received signals may be used to obtain the group velocity through

$$v_g(f) = \frac{d}{\text{T.O.F.}} \tag{6.1}$$

d being the distance traveled by the acoustic wave. In the transmission case this corresponds to the fixed distance between emitter and receiver, while in a reflected measurement it becomes $d = d_{emitter-defect} + d_{defect-receiver}$. The way the time of flight (T.O.F.) is obtained is clearly depicted in figure 6.4.

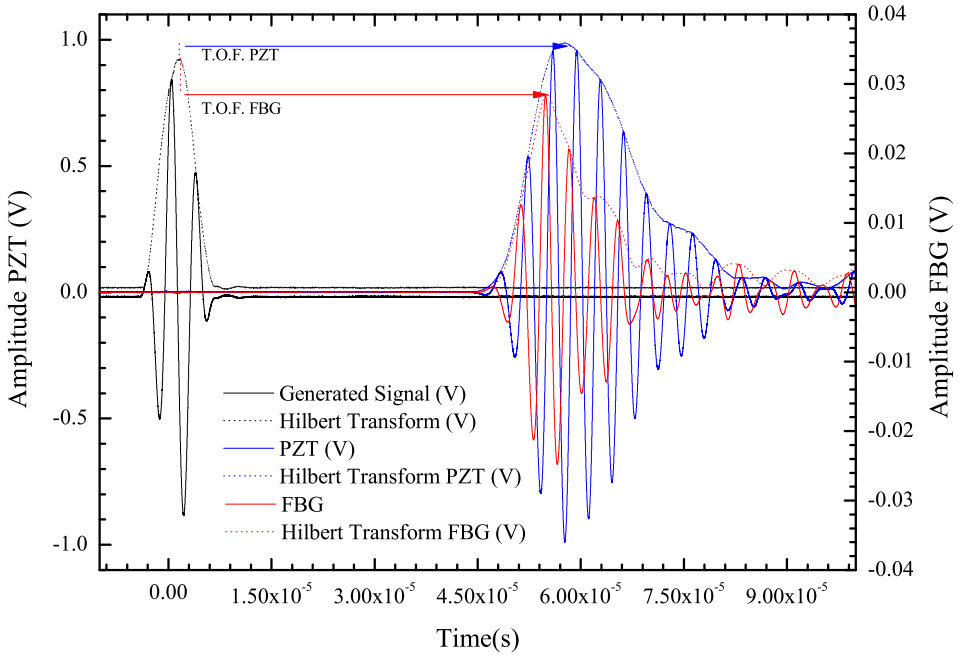

FIGURE 6.4: Example signals obtained after processing to reduce noise, and computing the Hilbert's transform. Data refers to 270kHz emission, and the maximum peak corresponds to the S0 mode.

6.3 Results

6.3.1 Dispersion Curves

In order to predict each emitted wave's group velocity, the dispersion curves for the composite plate were simulated, using MatLab code provided by the Laboratory for Active Materials and Smart Structures of the University of South Carolina (Figure 6.5).

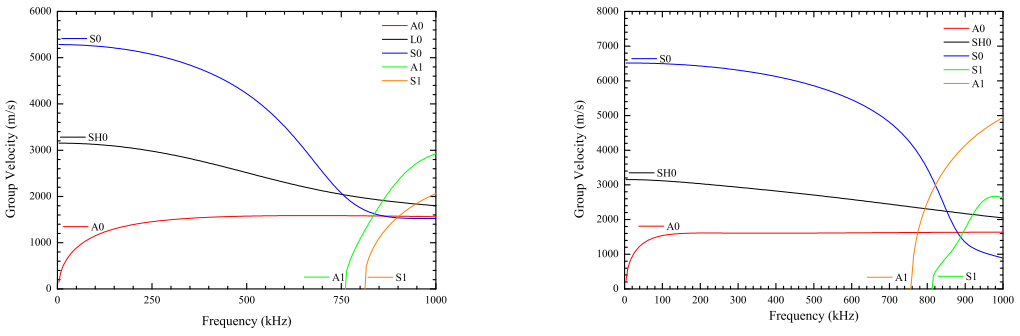

(A) Longitudinal propagation.

(B) Transverse propagation.

FIGURE 6.5: Dispersion curves (v_g) simulated for the used plate.

The simulation was done using the following a standard stiffness matrix (equation 6.2, characterized for a similar plate), for 0^o (Transverse) and 90^o (Longitudinal) emissions, with lamina density $1800kg/m^3$. The first two symmetric and anti-symmetric modes were plotted, as well as the first shear mode. The S0 and A0 modes are the most relevant as these are the ones more often used for damage detection (due to improved sensitivity derived from the lower frequencies).

$$\begin{bmatrix} 143.8 & 6.2 & 6.2 & 0 & 0 & 0 \\ 6.2 & 13.3 & 6.5 & 0 & 0 & 0 \\ 6.2 & 6.5 & 13.3 & 0 & 0 & 0 \\ 0 & 0 & 0 & 3.6 & 0 & 0 \\ 0 & 0 & 0 & 0 & 3.6 & 0 \\ 0 & 0 & 0 & 0 & 0 & 3.6 \end{bmatrix} GPa \tag{6.2}$$

6.3.2 FBG and PZT comparison

The following measurements show a comparison of the piezoelectric and FBG response to a emitted three-count burst with 90V peak-to-peak amplitude (Function generator connected to a x10 amplifier). Figures 6.6 present the measured group velocity over the simulated dispersion curves for both sensors in longitudinal and transverse emission.

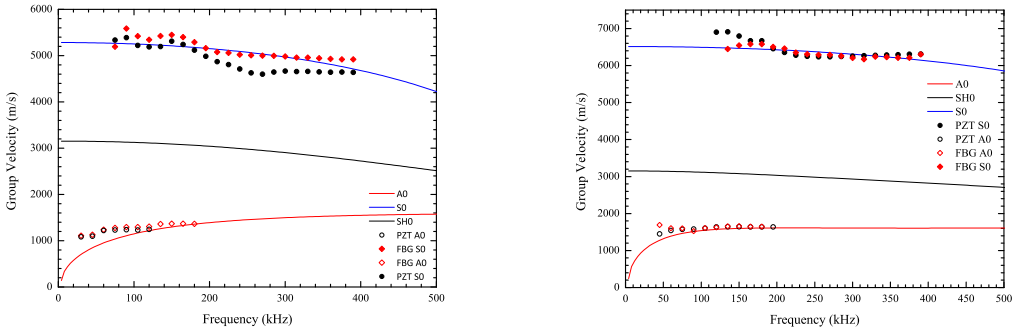

(A) Longitudinal emission. (B) Transverse emission.

FIGURE 6.6: Group velocities measured for the PZT and FBG.

which appear to be in good agreement, with clearly distinguishable A0 and S0 waves, some frequencies even producing measurable emissions of both modes. In general, though, lower frequencies seem to favor the anti-symmetric mode while higher frequencies favor the symmetric mode. This can be further confirmed in Figures 6.7, which plot the amplitudes of the previous measured emissions as a function of frequency, for each of the modes, for both sensors.

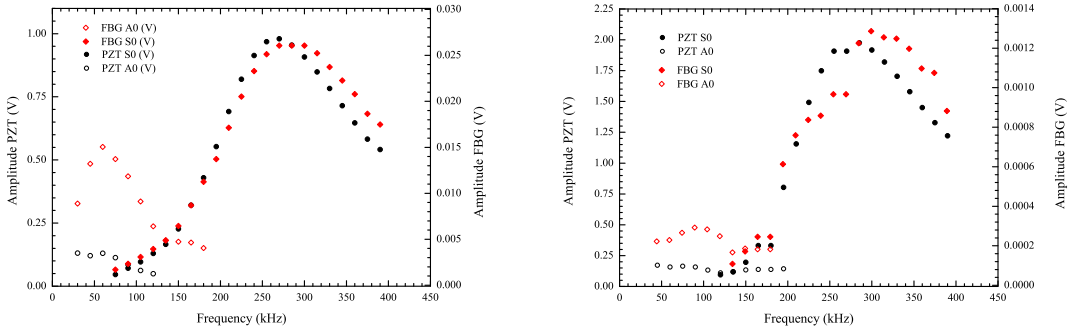

(A) Longitudinal emission. (B) Transverse emission.

FIGURE 6.7: Amplitude measured by the PZT and FBG sensors.

TABLE 6.1: Longitudinal emission maximum amplitude frequencies for each mode (f_{max}).

FBG		**PZT**	
A_0	S_0	A_0	S_0
60 kHz	280 kHz	60 kHz	280 kHz

From here, the maximum amplitude frequencies for the A0 wave mode and the S0 mode are clearly discriminated. It is also noteworthy that the FBG is relatively more sensitive to the A0 mode than the piezoelectric, especially in longitudinal emission. Also, the S0 mode amplitude is generally higher than that of the A0 mode.

The maximum sensitivity frequencies for longitudinal emission, for each mode, are presented in Table 6.1.

Also noteworthy, is that while the amplitude of the PZT (without any orientation) is greater for the transverse emission case (likely due to the inherent anisotropy of the composite plate, and different attenuations with the direction), that is not the case for the FBG. This is to be expected, as FBGs are most sensitive to longitudinal strains along the fiber, so longitudinal emissions should have improved sensitivity.

The FBG sensitivities for transverse and longitudinal emission are compared in Figure 6.8.

The longitudinal emission's amplitude is one order of magnitude greater than the transverse emission amplitude. Additionally, the increased relative sensitivity to the A0 mode previously noted is not as pronounced in the transverse emission case as it is in the longitudinal.

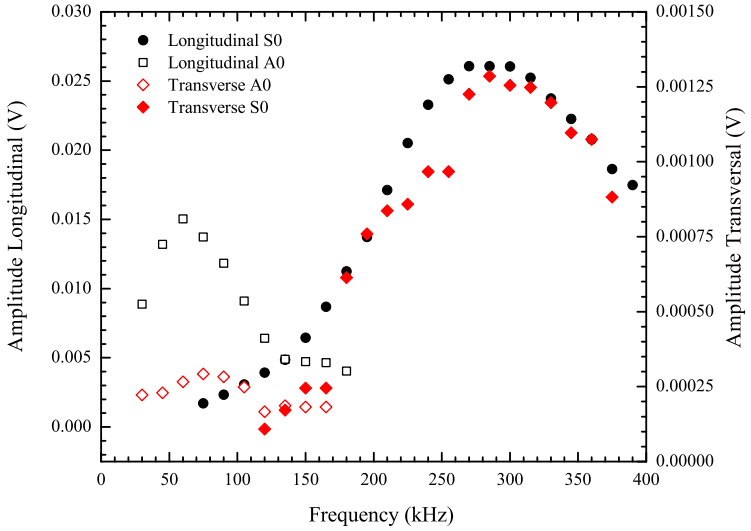

FIGURE 6.8: Comparison of the measured signal by the FBG for waves propagated longitudinally and transverse to the optical fiber.

6.3.3 Damage detection

For the damage detection, the first step is to establish the parameter to quantify damage. This is done by measuring a baseline of the plate prior to the introduction of the simulated defect, which is later used to calculate the severity of the defect.

Therefore a damage index is introduced, defined as

$$D.I. = \frac{\text{Amplitude}_{baseline} - \text{Amplitude}_{defect}}{\text{Amplitude}_{baseline}} \tag{6.3}$$

The sensitivity to damage is first correlated to the frequency of the propagated wave, in Figure 6.9.

From here, it is apparent that the A0 mode is the most sensitive to damage, with it's sensitivity maximum f'^{A0}_{max} being the same as the maximum of amplitude for the A0 mode, $f^{A0}_{max} = 60$ kHz (See Table 6.1). The S0 mode is noticeably less sensitive to damage. This is to be expected, as previous studies [102] have shown that the A0 mode is more sensitive to surface defects, while the S0 is better for the detection of damage through the thickness, despite their higher attenuation coefficients (hence the lower amplitude measured).

The defect was then moved displaced in 5 degree angle increments in relation to the wave emitter. The distance to the emitter was kept constant at 130mm. The frequency

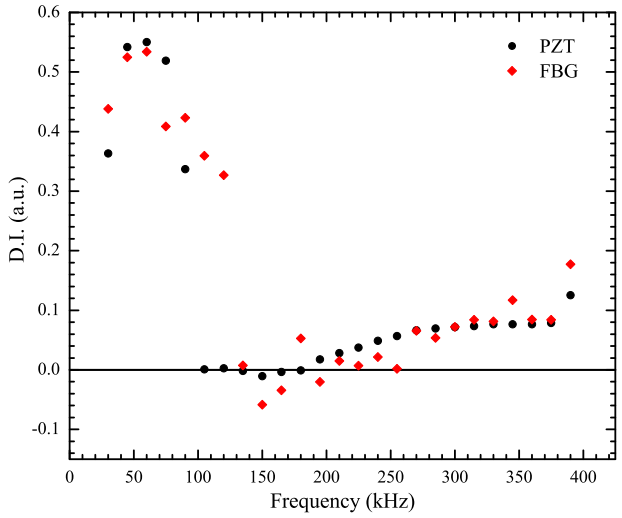

FIGURE 6.9: Damage index as a function of the frequency of the emitted wave.

was fixed at 60 kHz as it exhibited the maximum sensitivity to this kind of defect. The results are presented in Figure 6.10

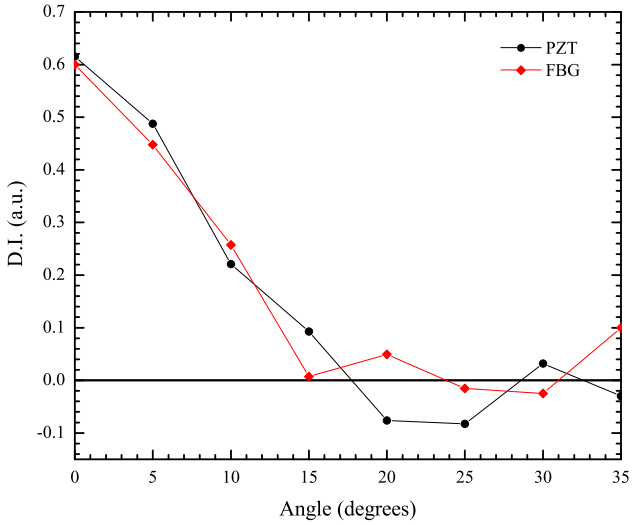

FIGURE 6.10: Damage index as a function of the angle of defect.

The FBG and PZT showed similar results. The defect was detectable up to 10 degrees with the FBG and up to 15 degrees with the piezoelectric, exhibiting an approximately linear reduction in amplitude with the angle displacement.

Part IV

Discussion and Conclusion

CHAPTER 7

Discussion and Conclusions

7.1 Discussion and Conclusions

The work showed promising results for fiber Bragg gratings as solutions for the embedding and manufacture of smart composites. These sensors were shown to be able to fill multiple roles of characterization and study of the material, in the form of manufacture monitoring, real-time monitoring of operation, and detection of damage and defects for assessment of a structure's integrity, while producing minimal influence on the local material's properties. A novel sensing head based on embedded fiber Bragg gratings for simultaneous measurements of physical parameters was designed. Experimental setups for each of the experiments were successfully designed, and comparisons with more standard methods were established. The viability of embedding techniques of the sensors was also assessed and analyzed.

Three hybrid-design (half unidirection, half bidirectional) CFRP plates with embedded fiber Bragg gratings were successfully manufactured through vacuum assisted resin infusion. Three samples were manufactured, revealing the most reliable method for manufacture to be by egressing through the edge of the composite, effectively reducing the chances of sensor break during the debagging process, despite preventing major reshaping and tooling of the composite after the lay-up and cure. Prior to infusion and cure, the sample was cut to a size close to the final test piece, allowing minimal handling post-cure, and reducing the need to use tools that could possibly endanger the sensor inlets for refining the shape. It is noteworthy that, as represented on the simulated models, the interface produced at the divide between unidirectional and bidirectional reinforcement of the sample produces a clear non-linear strain and stress behavior which may be interesting to study further.

The cure and manufacturing of the samples was monitored by the embedded sensors. The glass transition was verified to occur at $100C$ and $120C$ for the third, and the first two samples respectively. The reason for the shift may be attributed to differences in the chemical integrity of the resin, and more prolonged cup life (after mixture with the hardener) prior to the oven cure. The residual strains resulting in the sample were also assessed, showing high compressive strains (from $470\mu\varepsilon$ to $583\mu\varepsilon$) in the bidirectional section, and almost no residual strain ($52\mu\varepsilon$ tensile strain, and $16\mu\varepsilon$ compressive strain) on the unidirectional section. This effect is in accordance with previous studies which shown greater residual strains along the transverse direction of unidirectional composites, which suggests that the least longitudinally reinforced section should experience the most residual strains, as observed.

The tested samples response to the quasi-static mechanical tension and bending tests showed remarkable agreement with the previously FE simulated model for the strain and curvature measurements. These results, although tested only for a CFRP sample, should be analogous in other host materials, such as glass reinforced composites, since the design of the sensor head has it's functioning principle only on the relative properties of the sensors of each pair, altered by the lamina stack orientation. By embedding the FBG sensors, the temperature and strain/curvature response of each one in the pair was altered in relation to the surrounding local material properties of the composite materials. The thermal sensitivity for the FBG embedded at the bidirectional interface increased 49.6%, while the FBG at the unidirectional section remained constant, so the FBG sensitivities were shown to increase when embedded at a bidirectional interface. Meanwhile, the sensor embedded at the most longitudinal reinforced unidirectional section saw a reduction of it's strain sensitivity, while the sensor at the bidirectional section saw an expected increase, of the same magnitude, of around 23%. The accuracy of the sensor head may be able to be improved through further reducing the longitudinal reinforment along the bidirectional layer, thus increasing the difference in the strain sensitivities and increasing the determinant of the sensor matrix, or by solving the thermal sensitivity shift during the manufacture. In summary, a new sensing head based on embedded fibre Bragg gratings on composite plates was designed. The sensing head was experimentally tested and compared against results simulated through finite elements methods, with good agreement. The obtained results make it possible to obtain temperature and strain/curvature measurements simultaneously. By embedding the FBG sensors in the part to interrogate, the optical fibre is protected from damage and moisture. Temperature and strain sensitivities both change when embedded at a bidirectional interface, while unidirectional embedded sensors keep the thermal sensitivity.

The second part of the experimental work, in damage detection through acoustic sensing, consisted in the use of a composite quasi-isotropic CFRP plate with bonded sensors

for the propagation of longitudinal Lamb waves. The plate's group velocity dispersion curves were numerically estimated prior to the experiments, and good correlation was observed on the excited modes and their group velocity, compared to the calculated for the plate. A system for high acquisiton rate using FBGs was successfully designed using a tunable laser, optical circulator and photodetector. The FBG acquired signal was characterized for longitudinal and transverse emission, seeing a reduction of sensitivity of around one order of magnitude for transverse, compared to the longitudinal. The signal was also compared to that of piezoelectric sensors, which are more established. FBG and PZT sensors showed similar responses, with the FBG showing a relatively greater sensitivity to the first anti-symmetric mode of propagation, especially in longitudinal emission. The PZT also showed greater amplitudes for transverse emission, likely due to the inherent anisotropy of carbon fiber reinforced composite plates.

The setup was then assessed for the detection of a simulated defect. A 5 pence coin was used as a simulated circular defect and coupled to the plate. A damage index was defined in order to quantify the sensitivity to damage. The A0 mode was shown to be more sensitive to this kind of defects, having it's maximum amplitude at $60kHz$ emission. Since the defect was bonded to the surface, this is in accordance with previous studies which predict the A0 mode to have higher sensitivity than symmetric modes to surface defects. The defect was then changed in position, to see how it influences the measured damage index. Damage was found to be able to be detected up to 10-15 degrees off axis of the emitter and receptor transducers.

7.2 Proposed Future Work

Having the proposed discussed objectives being completed, the outcome of this work raises further questions and interesting studies which may be done in the future.

- Sample manufacturing and sensor embedding:
  - Study viable alternatives and improvements to the embedding process for vacuum assisted resin infusion
  - Attempt to use peel ply and tape to prevent the adhesion of the egress region to the composite, for out-of-plane ingress applications, in order to reduce the chance of breaking during the debagging.
- Cure monitoring of the sample:
  - Analyze the residual strain formation and glass transition strain behavior in the transverse direction with transverse aligned sensors.

  - Study the formation of residual strains through the thickness and at the interface region in the center.
  - Further study the glass transition strain behavior measured by the sensors.
  - Use other reference methods to assess the impact of the sensitivity change of the embedded sensors on the final measurements of residual strain.

- Simultaneous measurement of strain and temperature:

  - Study the strain behavior of the sample at the interface region.
  - Analyze the influence of the embedded sensor's and ingress/egress mechanism in the ultimate composite properties.
  - Attempt other plate designs, with different geometries, and compare the sensitivity and properties for sensing applications.

- Acoustic detection of damage:

  - Improve the optical measurement signal to noise ratio by using a light source able to lock-in to the FBG peak, and remove low-frequency temperature oscillations. This may also enable FBG use in passive acoustic emission sensing of damage formation and propagation, as the temperature random oscillations will stop triggering hits.
  - Compare the sensitivity of A0 and S0 modes for surface bonded and embedded FBGs, and their viability for assessing damage.
  - Study other kinds of defects, varying size, geometry, and position, and assessing the sensitivity of FBG to damage.
  - Attempt to locate damage by measurement of the reflected wave using an array of sensor.

APPENDIX A

Other sensors

A.1 Piezoelectrics

The piezoelectric effect refers to materials which produce an electrical field in response to a mechanical change, such as compression. Piezoelectric effect works both directly if the deformation creates an electric field, or inversely if the material is proportionally strained by an applied electric field. The most common piezoelectric material for transducers is Lead Zirconate Titanate, PbZrTi (PZT), although piezo-polymers and composites also see some application. Through application of an AC field, the PZT will vibrate at the same frequency as the applied voltage. Conversely, a mechanical oscillation will produce a voltage with the same frequency and of proportional amplitude. The applications of this kind of materials range from sensing and actuation [122], to power harvesting [123] Due to the reversible nature of the piezoelectric effect, PZT's in SHM and NDE applications can be used for passive (e.g. Acoustic Emission) and active (e.g. Guided Waves) implementations, as a transducer, emitter or actuator.

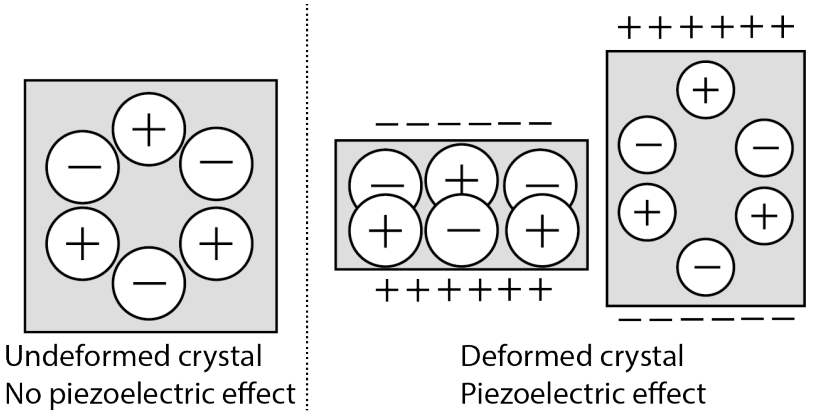

FIGURE A.1: Representation of the piezoelectric effect.

The piezoelectric effect is closely related to the crystallography symmetry of the material. Specifically, all components of the piezoelectric sensor vanish for centrosymmetric crystal structures. For noncentrosymmetric crystals, the piezoelectricity manifests by changing the magnitude or direction of the polarization vector through application of a mechanical load.

A.2 Thermocouples

Thermocouples are used as temperature measurement devices, made by joining two metal wires of different materials at both ends to create two junctions. One of the junctions, is connected to the body whose temperature is to be interrogated, while the other (called the cold junction) is connected to a reference temperature (usually a ice bath). As such, a thermal gradient is created between the reference and measurement junctions. This thermal gradient creates a movement of charge carriers due to Seebeck effect (i.e. thermoelectric effect) along each wire. Since the wires are composed of different materials, the experienced amount of thermoelectric effect in each wire will be different, effectively creating a current flow in the loop formed by both wires, that correlates to the measured temperature gradient.

By measuring the voltage generated between both junctions, it is possible to determine the temperature difference. Thermocouples come in many types, depending on the pair of metals in its composition, which may be used for different applications and temperature ranges. One of the most cheap, general purpose and commonly used (including in this work) is the type K thermocouple, made with a junction of chromel-alumel.

Bibliography

[1] J. M. Lopez-higuera, "Introduction to Fibre Optic Sensing Technology," in *Handbook of Optical Fibre Sensing Technology*, pp. 1–22, 2002.

[2] K. Shivakumar and L. Emmanwori, "Mechanics of failure of composite laminates with an embedded fiber optic sensor," *Journal of composite materials*, vol. 38, no. 8, pp. 669–680, 2004.

[3] D. W. Jensen, "Integrity of composite structures with embedded optical fibers," *Fiber optic smart structures(A 95-34976 09-39), New York, NY, John Wiley & Sons, Inc.(Wiley Series in Pure and Applied Optics), 1995,*, pp. 109–119, 1995.

[4] A. P. Strong, G. Lees, A. H. Hartog, R. Twohig, K. Kader, G. Hilton, S. Mullens, A. Khlybov, N. Sanderson, *et al.*, "An integrated system for pipeline condition monitoring," in *International Petroleum Technology Conference*, International Petroleum Technology Conference, 2009.

[5] K. S. C. Kuang, R. Kenny, M. P. Whelan, W. J. Cantwell, and P. R. Chalker, "Embedded fibre Bragg grating sensors in advanced composite materials," *Composites Science and Technology*, vol. 61, no. 10, pp. 1379–1387, 2001.

[6] W. Jin, "Multiplexed FBG sensors and their applications," *Proc. SPIE Vol. 3897*, vol. 3897, pp. 468–479, 1999.

[7] J. Leng and A. Asundi, "Structural health monitoring of smart composite materials by using efpi and fbg sensors," *Sensors and Actuators, A: Physical*, vol. 103, no. 3, pp. 330–340, 2003.

[8] H.-K. Kang, D.-H. Kang, H.-J. Bang, C.-S. Hong, and C.-G. Kim, "Cure monitoring of composite laminates using fiber optic sensors," *Smart Materials and Structures*, vol. 11, no. 2, pp. 279–287, 2002.

[9] J. M. Balvers, *In situ strain & cure monitoring in liquid composite moulding by fibre Bragg grating sensors door*. 2014.

[10] M. S. Ferreira, J. Vieira, C. Frias, and O. Frazão, "Simultaneous measurement of strain and temperature using fiber Bragg grating sensors embedded in hybrid composite laminates," *Measurement Science and Technology*, vol. 22, no. 4, p. 045206, 2011.

[11] C. Doyle, A. Martin, T. Liu, M. Wu, S. Hayes, P. A. Crosby, G. R. Powell, D. Brooks, and G. F. Fernando, "In-situ process and condition monitoring of advanced fibre-reinforced composite materials using optical fibre sensors," *Smart Materials and Structures*, vol. 7, no. 2, p. 145, 1998.

[12] L. Rodriguez-Cobo, A. Marques, J. López-Higuera, J. Santos, and O. Frazao, "New design for temperature–strain discrimination using fiber bragg gratings embedded in laminated composites," *Smart Materials and Structures*, vol. 22, no. 10, p. 105011, 2013.

[13] V. Giurgiutiu, C. Roman, B. Lin, and E. Frankforter, "Omnidirectional piezo-optical ring sensor for enhanced guided wave structural health monitoring," *Smart Materials and Structures*, vol. 24, no. 1, p. 015008, 2015.

[14] I. M. Perez, H. Cui, and E. Udd, "Acoustic emission detection using fiber bragg gratings," 2001.

[15] A. Propst, K. Peters, M. A. Zikry, S. Schultz, W. Kunzler, Z. Zhu, M. Wirthlin, and R. Selfridge, "Assessment of damage in composite laminates through dynamic, full-spectral interrogation of fiber bragg grating sensors," *Smart Materials and Structures*, vol. 19, no. 1, p. 015016, 2010.

[16] I. McKenzie, R. Jones, I. H. Marshall, and S. Galea, "Optical fibre sensors for health monitoring of bonded repair systems," *Composite Structures*, vol. 50, no. 4, pp. 405–416, 2000.

[17] R. Gibson, *Principles of Composite Material Mechanics, Third Edition*. Mechanical Engineering, Taylor & Francis, 2011.

[18] K. Chawla, *Composite Materials: Science and Engineering*. Springer.

[19] K. Chawla, "3 matrix materials," in *Composite Materials: Science and Engineering*, Springer.

[20] K. Chawla, "2 reinforcements," in *Composite Materials: Science and Engineering*, Springer.

[21] E. Barbero, *Introduction to Composite Materials Design, Second Edition*.

[22] A. Standard, "D3171-09," *Standard test methods for constituent content of composite materials, ASTM International, West Conshohocken (PA)*, 2009.

[23] K. Chawla, "10 micromechanics of composites," in *Composite Materials: Science and Engineering*, Springer.

[24] E. Barbero, *Introduction to Composite Materials Design, Second Edition*.

[25] K. Chawla, "11 macromechanics of composites," in *Composite Materials: Science and Engineering*, Springer.

[26] R. B. Heslehurst, "2 damage and defect description - appendix a," in *Defects and Damage in Composite Materials and Structures*.

[27] R. B. Heslehurst, "5 loss of integrity," in *Defects and Damage in Composite Materials and Structures*.

[28] R. B. Heslehurst, "4 failure mechanisms," in *Defects and Damage in Composite Materials and Structures*.

[29] B. Lee, "Review of the present status of optical fiber sensors," *Optical Fiber Technology*, vol. 9, no. 2, pp. 57–79, 2003.

[30] G. Zhou and L. Sim, "Evaluating damage in smart composite laminates using embedded efpi strain sensors," *Optics and Lasers in Engineering*, vol. 47, no. 10, pp. 1063–1068, 2009.

[31] H. Murayama, K. Kageyama, H. Naruse, A. Shimada, and K. Uzawa, "Application of fiber-optic distributed sensors to health monitoring for full-scale composite structures," *Journal of Intelligent Material Systems and Structures*, vol. 14, no. 1, pp. 3–13, 2003.

[32] H. Xiao, J. Deng, G. Pickrell, R. G. May, and A. Wang, "Single-crystal sapphire fiber-based strain sensor for high-temperature applications," *Journal of lightwave technology*, vol. 21, no. 10, p. 2276, 2003.

[33] J. Zubia and J. Arrue, "Plastic optical fibers: An introduction to their technological processes and applications," *Optical Fiber Technology*, vol. 7, no. 2, pp. 101–140, 2001.

[34] C. Chen, *Foundations for Guided-Wave Optics*. Wiley, 2006.

[35] K. O. Hill and G. Meltz, "Fiber bragg grating technology fundamentals and overview," *Journal of lightwave technology*, vol. 15, no. 8, pp. 1263–1276, 1997.

[36] W. W. Morey, G. Meltz, and W. H. Glenn, "Fiber optic bragg grating sensors," in *OE/FIBERS'89*, pp. 98–107, International Society for Optics and Photonics, 1990.

[37] A. D. Kersey, M. A. Davis, H. J. Patrick, M. LeBlanc, K. Koo, C. Askins, M. Putnam, and E. J. Friebele, "Fiber grating sensors," *Journal of lightwave technology*, vol. 15, no. 8, pp. 1442–1463, 1997.

[38] K. Hill, Y. Fujii, D. C. Johnson, and B. Kawasaki, "Photosensitivity in optical fiber waveguides: Application to reflection filter fabrication," *Applied Physics Letters*, vol. 32, no. 10, pp. 647–649, 1978.

[39] G. Meltz, W. Morey, and W. Glenn, "Formation of bragg gratings in optical fibers by a transverse holographic method," *Optics letters*, vol. 14, no. 15, pp. 823–825, 1989.

[40] G. Meltz, W. Morey, and W. Glenn, "Formation of bragg gratings in optical fibers by a transverse holographic method," *Optics letters*, vol. 14, no. 15, pp. 823–825, 1989.

[41] K. O. Hill, B. Malo, F. Bilodeau, D. Johnson, and J. Albert, "Bragg gratings fabricated in monomode photosensitive optical fiber by uv exposure through a phase mask," *Applied Physics Letters*, vol. 62, no. 10, pp. 1035–1037, 1993.

[42] W. Du, X. Tao, H. Tam, and C. Choy, "Fundamentals and applications of optical fiber bragg grating sensors to textile structural composites," *Composite Structures*, vol. 42, no. 3, pp. 217–229, 1998.

[43] T. Erdogan, "Fiber grating spectra," *Lightwave Technology, Journal of*, vol. 15, no. 8, pp. 1277–1294, 1997.

[44] B. Malo, K. O. Hill, F. Bilodeau, D. Johnson, and J. Albert, "Point-by-point fabrication of micro-bragg gratings in photosensitive fibre using single excimer pulse refractive index modification techniques," *Electronics Letters*, vol. 29, no. 18, pp. 1668–1669, 1993.

[45] R. Kashyap, *Fiber Bragg Gratings*. Electronics & Electrical, Academic Press, 1999.

[46] C. Doyle, "Fibre bragg grating sensors-an introduction to bragg gratings and interrogation techniques," *Smart Fibres Ltd*, pp. 1–5, 2003.

[47] A. D. Eric Udd, James S. Sirkis, "4 optical fiber/composite interaction mechanics," in *Fiber Optic Smart Structures*, pp. 61–109, Wiley-Interscience, 1995.

[48] A. Dasgupta, Y. Wan, J. S. Sirkis, and H. Singh, "Micromechanical investigation of an optical fiber embedded in a laminated composite," in *San Jose-DL tentative*, pp. 119–128, International Society for Optics and Photonics, 1990.

[49] D. Lee, J. Lee, and S. Yun, "The mechanical characteristics of smart composite structures with embedded optical fiber sensors," *Composite Structures*, vol. 32, no. 1, pp. 39–50, 1995.

[50] B. Benchekchou and N. Ferguson, "The effect of embedded optical fibres on the fatigue behaviour of composite plates," *Composite structures*, vol. 41, no. 2, pp. 113–120, 1998.

[51] S. S. Roberts and R. Davidson, "Mechanical properties of composite materials containing embedded fiber-optic sensors," in *OE Fiber-DL tentative*, pp. 326–341, International Society for Optics and Photonics, 1991.

[52] L. G. Melin, K. Levin, S. Nilsson, S. Palmer, and P. Rae, "A study of the displacement field around embedded fibre optic sensors," *Composites Part A: Applied Science and Manufacturing*, vol. 30, no. 11, pp. 1267–1275, 1999.

[53] E. Udd, "2 fiber optic smart structure technology," in *Fiber Optic Smart Structures*, pp. 5–23, Wiley-Interscience, 1995.

[54] A. Dasgupta and J. S. Sirkis, "Importance of coatings to optical fiber sensors embedded in'smart'structures," *AIAA journal*, vol. 30, no. 5, pp. 1337–1343, 1992.

[55] J. S. Sirkis and A. Dasgupta, "Optimal coatings for intelligent structure fiber optic sensors," in *San Jose-DL tentative*, pp. 129–140, International Society for Optics and Photonics, 1990.

[56] J. R. L. Eric Udd, William B. Spillman Jr., "6 methods of fiber optic ingress/egress for smart structures," in *Fiber Optic Smart Structures*, pp. 121–155, Wiley-Interscience, 1995.

[57] D. G. Lee, M. Mitrovic, A. Friedman, G. P. Carman, and L. Richards, "Characterization of fiber optic sensors for structural health monitoring," *Journal of composite materials*, vol. 36, no. 11, pp. 1349–1366, 2002.

[58] P. Schubel, R. Crossley, E. Boateng, and J. Hutchinson, "Review of structural health and cure monitoring techniques for large wind turbine blades," *Renewable Energy*, vol. 51, pp. 113–123, 2013.

[59] C. M. Lawrence, D. V. Nelson, T. E. Bennett, and J. R. Spingarn, "An embedded fiber optic sensor method for determining residual stresses in fiber-reinforced composite materials," *Journal of intelligent material systems and structures*, vol. 9, no. 10, pp. 788–799, 1998.

[60] J.-Y. Chen, S. Hoa, C.-K. Jen, and H. Wang, "Fiber-optic and ultrasonic measurements for in-situ cure monitoring of graphite/epoxy composites," *Journal of composite materials*, vol. 33, no. 20, pp. 1860–1881, 1999.

[61] K. Osaka, T. Kosaka, Y. Asano, and T. Fukuda, "Measurement of internal strains in frp laminate with efpi optical fiber sensor during autoclave molding; measurement in off-axis directions," in *Proceedings of the Second Asian-Australasian Conference on Composite Materials (ACCM-2000)*, pp. 1117–1122, Kyongju, Korea, 2000.

[62] G. F. Fernando, "Fibre optic sensor systems for monitoring composite structures," *Reinforced Plastics*, vol. 49, no. 11, pp. 41–49, 2005.

[63] A. Aktas, S. Boyd, and R. Shenoi, "Cure and strain monitoring of novel unsaturated polyester/phenolic resin blends in the vacuum infusion process using fibre bragg gratings," *Journal of Composite Materials*, p. 0021998314568165, 2015.

[64] K. Vijaya Kumar, M. Safiulla, and A. Khaleel Ahmed, "Analysis of vacuum failures during curing of cfrp composites," *International Journal Of Scientific & Technology Research*, vol. 2, no. 5, pp. 220–225, 2013.

[65] D. Karalekas, J. Cugnoni, and J. Botsis, "Monitoring of process induced strains in a single fibre composite using fbg sensor: A methodological study," *Composites Part A: Applied Science and Manufacturing*, vol. 39, no. 7, pp. 1118–1127, 2008.

[66] L. Khoun, R. de Oliveira, V. Michaud, and P. Hubert, "Investigation of process-induced strains development by fibre bragg grating sensors in resin transfer moulded composites," *Composites Part A: Applied Science and Manufacturing*, vol. 42, no. 3, pp. 274–282, 2011.

[67] R. De Oliveira, S. Lavanchy, R. Chatton, D. Costantini, V. Michaud, R. Salathé, and J.-A. Månson, "Experimental investigation of the effect of the mould thermal expansion on the development of internal stresses during carbon fibre composite processing," *Composites Part A: Applied Science and Manufacturing*, vol. 39, no. 7, pp. 1083–1090, 2008.

[68] H. Hahn, "Effects of residual stresses in polymer matrix composites," *Journal of the Astronautical Sciences*, vol. 32, pp. 253–267, 1984.

[69] H.-K. Kang, D.-H. Kang, H.-J. Bang, C.-S. Hong, and C.-G. Kim, "Cure monitoring of composite laminates using fiber optic sensors," *Smart materials and structures*, vol. 11, no. 2, p. 279, 2002.

[70] Z.-S. Guo, "Strain and temperature monitoring of asymmetric composite laminate using fbg hybrid sensors," *Structural Health Monitoring*, vol. 6, no. 3, pp. 191–197, 2007.

[71] J. Leng and A. Asundi, "Real-time cure monitoring of smart composite materials using extrinsic fabry-perot interferometer and fiber bragg grating sensors," *Smart materials and structures*, vol. 11, no. 2, p. 249, 2002.

[72] J. Leng and A. Asundi, "Structural health monitoring of smart composite materials by using efpi and fbg sensors," *Sensors and Actuators A: Physical*, vol. 103, no. 3, pp. 330–340, 2003.

[73] V. Murukeshan, P. Chan, L. Ong, and L. Seah, "Cure monitoring of smart composites using fiber bragg grating based embedded sensors," *Sensors and Actuators A: Physical*, vol. 79, no. 2, pp. 153–161, 2000.

[74] P. P. Parlevliet, E. Voet, H. E. Bersee, and A. Beukers, "Process monitoring with fbg sensors during vacuum infusion of thick composite laminates," in *16th International conference on Composite Materials*, 2007.

[75] M. Harsch, J. Karger-Kocsis, and F. Herzog, "Influence of cure regime on the strain development in an epoxy resin as monitored by a fiber bragg grating sensor," *Macromolecular Materials and Engineering*, vol. 292, no. 4, pp. 474–483, 2007.

[76] F. Colpo, L. Humbert, and J. Botsis, "Characterisation of residual stresses in a single fibre composite with fbg sensor," *Composites Science and Technology*, vol. 67, no. 9, pp. 1830–1841, 2007.

[77] K. Kuang, R. Kenny, M. Whelan, W. Cantwell, and P. Chalker, "Embedded fibre bragg grating sensors in advanced composite materials," *Composites Science and Technology*, vol. 61, no. 10, pp. 1379–1387, 2001.

[78] J. A. Epaarachchi, J. Canning, and M. Stevenson, "The response of embedded nir (830 nm) fiber bragg grating sensors in glass composites under fatigue loading," *Journal of composite materials*, 2009.

[79] G. C. Kahandawa, J. Epaarachchi, H. Wang, and K. Lau, "Use of fbg sensors for shm in aerospace structures," *Photonic Sensors*, vol. 2, no. 3, pp. 203–214, 2012.

[80] H. Davies, L. A. Everall, and A. M. Gallon, "Application of smart optical fiber sensors for structural load monitoring," in *SPIE's 8th Annual International Symposium on Smart Structures and Materials*, pp. 114–123, International Society for Optics and Photonics, 2001.

[81] H. Patrick, G. Williams, A. Kersey, J. Pedrazzani, and A. Vengsarkar, "Hybrid fiber bragg grating/long period fiber grating sensor for strain/temperature discrimination," *Photonics Technology Letters, IEEE*, vol. 8, no. 9, pp. 1223–1225, 1996.

[82] S. James, M. Dockney, and R. Tatam, "Simultaneous independent temperature and strain measurement using in-fibre bragg grating sensors," *Electronics Letters*, vol. 32, no. 12, pp. 1133–1134, 1996.

[83] B.-O. Guan, H.-Y. Tam, X.-M. Tao, and X.-Y. Dong, "Simultaneous strain and temperature measurement using a superstructure fiber bragg grating," *Photonics Technology Letters, IEEE*, vol. 12, pp. 675–677, June 2000.

[84] B.-O. Guan, H.-Y. Tam, S.-L. Ho, W.-H. Chung, and X.-Y. Dong, "Simultaneous strain and temperature measurement using a single fibre bragg grating," *Electronics Letters*, vol. 36, no. 12, pp. 1018–1019, 2000.

[85] F. Peng, Z. Ran, Y. Rao, and Y. Liu, "A hybrid Raman/FBG sensing system for simultaneous measurement of temperature and strain," in *22nd International Conference on Optical Fiber Sensors*, vol. 8421, 2012.

[86] W. Urbanczyk, E. Chmielewska, and W. J. Bock, "Measurements of temperature and strain sensitivities of a two-mode bragg grating imprinted in a bow-tie fibre," *Measurement Science and Technology*, vol. 12, no. 7, p. 800, 2001.

[87] M. Sudo, M. Nakai, K. Himeno, S. Suzaki, A. Wada, and R. Yamauchi, "Simultaneous measurement of temperature and strain using panda fiber grating," in *Optical Fiber Sensors*, p. OWC7, Optical Society of America, 1997.

[88] L. A. Ferreira, F. M. Arau, F. Farahi, *et al.*, "Simultaneous measurement of strain and temperature using interferometrically interrogated fiber bragg grating sensors," *Optical Engineering*, vol. 39, no. 8, pp. 2226–2234, 2000.

[89] W.-C. Du, X.-M. Tao, and H.-Y. Tam, "Fiber bragg grating cavity sensor for simultaneous measurement of strain and temperature," *Photonics Technology Letters, IEEE*, vol. 11, no. 1, pp. 105–107, 1999.

[90] J. Jung, H. Nam, J. H. Lee, N. Park, and B. Lee, "Simultaneous measurement of strain and temperature by use of a single-fiber bragg grating and an erbium-doped fiber amplifier," *Applied optics*, vol. 38, no. 13, pp. 2749–2751, 1999.

[91] J. Jung, N. Park, and B. Lee, "Simultaneous measurement of strain and temperature by use of a single fiber bragg grating written in an erbium: ytterbium-doped fiber," *Applied Optics*, vol. 39, no. 7, pp. 1118–1120, 2000.

[92] V. Spirin, M. Shlyagin, S. Miridonov, and I. Marquez, "Temperature-insensitive strain measurement using differential double bragg grating technique," *Optics & Laser Technology*, vol. 33, no. 1, pp. 43–46, 2001.

[93] M. Song, S. B. Lee, S. S. Choi, and B. Lee, "Simultaneous measurement of temperature and strain using two fiber bragg gratings embedded in a glass tube," *Optical Fiber Technology*, vol. 3, no. 2, pp. 194–196, 1997.

[94] O. Frazão, R. Oliveira, and I. Dias, "A simple smart composite using fiber bragg grating sensors for strain and temperature discrimination," *Microwave and Optical Technology Letters*, vol. 51, no. 1, pp. 235–239, 2009.

[95] M. Ferreira, J. Vieira, C. Frias, and O. Frazão, "Simultaneous measurement of strain and temperature using fiber bragg grating sensors embedded in hybrid composite laminates," *Measurement Science and Technology*, vol. 22, no. 4, p. 045206, 2011.

[96] D. Worlton, "Experimental confirmation of lamb waves at megacycle frequencies," *Journal of Applied Physics*, vol. 32, no. 6, pp. 967–971, 1961.

[97] J. Rose, *Ultrasonic Waves in Solid Media*. Cambridge University Press, 2004.

[98] J. L. Rose, "A baseline and vision of ultrasonic guided wave inspection potential," *Journal of pressure vessel technology*, vol. 124, no. 3, pp. 273–282, 2002.

[99] K. Worden, G. Manson, and D. Allman, "Experimental validation of a structural health monitoring methodology: Part i. novelty detection on a laboratory structure," *Journal of Sound and Vibration*, vol. 259, no. 2, pp. 323–343, 2003.

[100] E. A. Birt, "Damage detection in carbon-fibre composites using ultrasonic lamb waves," *Insight*, vol. 40, no. 5, pp. 335–339, 1998.

[101] W. Percival and E. A. Birt, "A study of lamb wave propagation in carbon-fibre composites," *Insight*, vol. 39, no. 10, pp. 728–735, 1997.

[102] Z. Su, L. Ye, and Y. Lu, "Guided lamb waves for identification of damage in composite structures: A review," *Journal of sound and vibration*, vol. 295, no. 3, pp. 753–780, 2006.

[103] P. Tua, S. Quek, and Q. Wang, "Detection of cracks in plates using piezo-actuated lamb waves," *Smart Materials and Structures*, vol. 13, no. 4, p. 643, 2004.

[104] P. Wilcox, M. Lowe, and P. Cawley, "Mode and transducer selection for long range lamb wave inspection," *Journal of intelligent material systems and structures*, vol. 12, no. 8, pp. 553–565, 2001.

[105] P. Wilcox, M. Lowe, and P. Cawley, "The effect of dispersion on long-range inspection using ultrasonic guided waves," *NDT & E International*, vol. 34, no. 1, pp. 1–9, 2001.

[106] B. Tang and E. I. HENNEKE, "Lamb-wave monitoring of axial stiffness reduction of laminated composite plates," *Materials Evaluation*, vol. 47, no. 8, pp. 928–934, 1989.

[107] M. D. Seale, B. T. Smith, and W. Prosser, "Lamb wave assessment of fatigue and thermal damage in composites," *The Journal of the Acoustical Society of America*, vol. 103, no. 5, pp. 2416–2424, 1998.

[108] L. Demer and L. Fentnor, "Lamb wave techniques in nondestructive testing(lamb waves behavior applied to defect evaluation in nondestructive tests of solid elongated cylindrical objects)," *International Journal of Nondestructive Testing*, vol. 1, pp. 251–283, 1969.

[109] D. A. Saravanos and P. R. Heyliger, "Coupled layerwise analysis of composite beams with embedded piezoelectric sensors and actuators," *Journal of Intelligent Material Systems and Structures*, vol. 6, no. 3, pp. 350–363, 1995.

[110] D. A. Saravanos, V. Birman, and D. A. Hopkins, "Detection of delaminations in composite beams using piezoelectric sensors," *NASA Technical Memorandum*, vol. 106611, 1994.

[111] R. Monkhouse, P. Wilcox, and P. Cawley, "Flexible interdigital pvdf transducers for the generation of lamb waves in structures," *Ultrasonics*, vol. 35, no. 7, pp. 489–498, 1997.

[112] R. Monkhouse, P. Wilcox, M. Lowe, R. Dalton, and P. Cawley, "The rapid monitoring of structures using interdigital lamb wave transducers," *Smart Materials and Structures*, vol. 9, no. 3, p. 304, 2000.

[113] S. Valdez, *Structural integrity monitoring of CFRP laminates using piezoelectric devices*. PhD thesis, Imperial College London (University of London), 2000.

[114] S. Diaz Valdes and C. Soutis, "Health monitoring of composites using lamb waves generated by piezoelectric devices," *Plastics, Rubber and Composites*, vol. 29, no. 9, pp. 475–481, 2000.

[115] S. Valdes and C. Soutis, "A structural health monitoring system for laminated composites," in *Proceedings of DETC*, pp. 2013–2020, 2001.

[116] J. G. Teixeira, I. T. Leite, S. Silva, and O. Frazão, "Advanced fiber-optic acoustic sensors," *Photonic Sensors*, vol. 4, no. 3, pp. 198–208, 2014.

[117] N. Miesen, Y. Mizutani, R. M. Groves, J. Sinke, and R. Benedictus, "Lamb wave detection in prepreg composite materials with fibre bragg grating sensors," in *SPIE Smart Structures and Materials+ Nondestructive Evaluation and Health Monitoring*, pp. 79812J–79812J, International Society for Optics and Photonics, 2011.

[118] S. S. Kessler, S. M. Spearing, and M. J. Atalla, "In-situ damage detection of composites structures using lamb wave methods," in *Proceedings of the First European Workshop on Structural Health Monitoring*, pp. 10–12, 2002.

[119] S. Pierce, W. Philp, A. Gachagan, A. McNab, G. Hayward, and B. Culshaw, "Surface-bonded and embedded optical fibers as ultrasonic sensors," *Applied optics*, vol. 35, no. 25, pp. 5191–5197, 1996.

[120] W. Jin, W. C. Michie, G. Thursby, M. Konstantaki, and B. Culshaw, "Simultaneous measurement of strain and temperature: error analysis," *Optical Engineering*, vol. 36, no. 2, pp. 598–609, 1997.

[121] G. Pereira, C. Frias, H. Faria, O. Frazão, and A. Marques, "On the improvement of strain measurements with fbg sensors embedded in unidirectional composites," *Polymer Testing*, vol. 32, no. 1, pp. 99–105, 2013.

[122] C. Y. Chee, L. Tong, and G. P. Steven, "A review on the modelling of piezoelectric sensors and actuators incorporated in intelligent structures," *Journal of Intelligent Material Systems and Structures*, vol. 9, no. 1, pp. 3–19, 1998.

[123] S. R. Anton and H. A. Sodano, "A review of power harvesting using piezoelectric materials (2003–2006)," *Smart materials and Structures*, vol. 16, no. 3, p. R1, 2007.